Fully implicit local time-stepping methods for advection-diffusion problems in mixed formulations

Thi-Thao-Phuong Hoang[a,1]

[a]*Department of Mathematics and Statistics, Auburn University, Auburn, AL 36849, USA.*

Abstract

This paper is concerned with numerical solution of transport problems in heterogeneous porous media. A semi-discrete continuous-in-time formulation of the linear advection-diffusion equation is obtained by using a mixed hybrid finite element method, in which the flux variable represents both the advective and diffusive flux, and the Lagrange multiplier arising from the hybridization is used for the discretization of the advective term. Based on global-in-time and nonoverlapping domain decomposition, we propose two implicit local time-stepping methods to solve the semi-discrete problem. The first method uses the time-dependent Steklov-Poincaré type operator and the second uses the optimized Schwarz waveform relaxation (OSWR) with Robin transmission conditions. For each method, we formulate a space-time interface problem which is solved iteratively. Each iteration involves solving the subdomain problems independently and globally in time; thus, different time steps can be used in the subdomains. The convergence of the fully discrete OSWR algorithm with nonmatching time grids is proved. Numerical results for problems with various Peclét numbers and discontinuous coefficients, including a prototype for the simulation of the underground storage of nuclear waste, are presented to illustrate the performance of the proposed local time-stepping methods.

Keywords: heterogeneous problems; advection–diffusion; mixed formulations; time-dependent Steklov-Poincaré; optimized Schwarz waveform relaxation; local time-stepping

1. Introduction

Numerical simulations of transport problems in heterogeneous porous media is a subject of great importance in science and engineering. For applications in hydrology, various geological layers with different hydrogeological properties are involved in the simulations. Consequently, the time scales may vary over several order of magnitudes across these

layers. This is particularly the case when one simulates the transport of contaminants in and around a nuclear waste repository. Clearly, using a single-time step size throughout the entire domain is computationally inefficient; instead, one should use different time steps in different parts of the domain depending on their physical properties. In addition, for the application we consider, large time step sizes are desirable due to the long time simulation as the nuclear waste decays very slowly. Therefore, we propose to use global-in-time, nonoverlapping domain decomposition (DD) methods in which the dynamic system is decoupled into dynamic subsystems defined on the subdomains (resulting from a spatial decomposition). Then time-dependent problems are solved implicitly in each subdomain at each iteration and the information is exchanged over the space-time interfaces between subdomains. As a consequence, different time steps can be used in the subdomains. For spatial discretization, we use mixed methods [12, 47] for their mass conservation property and satisfactory performance on heterogeneous problems. In addition, to handle advection-dominance problems, we employ the (upwind) mixed hybrid finite element method as proposed in [46, 13], in which the flux variable approximates the total flux (i.e. both diffusive and advective flux). It was shown that the new mixed hybrid method [46, 13] is fully mass conservative and as accurate as the standard mixed method [16], while it is more efficient in terms of computational cost and robust for problems with high Peclét numbers.

There are basically two types of global-in-time DD methods: the first approach is based on the physical transmission conditions, for example, the Dirichlet-Neumann and Neumann-Neumann waveform relaxation methods [41, 39, 27, 28]. The second approach is the Schwarz iteration based on more general transmission conditions such as Robin or Ventcell conditions; an important class of methods in this category is the Optimized Schwarz Waveform Relaxation (OSWR) algorithm where additional coefficients involved in the transmission conditions are optimized to improve convergence rates [24, 45, 21, 23, 9, 7, 30, 31, 32, 8, 29, 6]. Both approaches were studied with mixed formulations of the pure diffusion problem in [34] and the linear advection-diffusion problem in [37]. Particularly in [34], a global-in-time preconditioned Schur method (GTP-Schur) and a global-in-time optimized Schwarz method (GTO-Schwarz) were proposed. Space-time interface problems were derived using, for GTP-Schur, the time-dependent Dirichlet-to-Neumann (or Steklov-Poincaré) operator and, for GTO-Schwarz, the time-dependent Robin-to-Robin operator.

For the GTP-Schur method, the interface problem is solved by preconditioned GMRES with the time-dependent Neumann-Neumann preconditioner, extended from the Balancing Domain Decomposition (BDD) preconditioner for stationary problems which is known to be efficient when highly heterogeneous coefficients are present [42, 14, 43]. Advanced versions of BDD methods are Balancing Domain Decomposition by Constraints (BDDC) methods which introduce a global coarse problem to obtain the condition number bound when the number of subdomains increases (see, e.g., [15, 17, 19, 44, 49, 40, 11]).

For the GTO-Schwarz method, the interface problem is solved by either Jacobi iterations or GMRES. The former choice is equivalent to the OSWR algorithm with Robin transmission conditions, from which the optimized Robin parameters are computed by min-

2

imizing the convergence factor in the Fourier transform domain [21, 23, 7, 8]. The interface problems are in mixed form and are space-time for both GTP-Schur and GTP-Schwarz methods, thus nonconforming time grids are possible via a suitable L^2 projection in time. An optimal projection algorithm can be found in [24, 26, 25].

In [37], the two methods were extended to the case of advection-diffusion equations with *operator splitting* to treat advection and diffusion with different numerical schemes. For the temporal discretization, the advection is approximated with the explicit Euler method (where sub-time steps are used and constrained by the CFL condition) and the diffusion with the implicit Euler method. For the spatial discretization, both are approximated with locally mass conservative schemes: the advection with an upwind, cell-center finite volume scheme and the diffusion with a mixed finite element method. The discrete interface problems for the GTP-Schur and GTO-Schwarz methods are obtained by introducing new unknowns to enforce Dirichlet transmission conditions between subdomains for the advection step while the diffusion step is handled in the same manner as in [34]. In other words, the transmission conditions for the advection part and the diffusion part are separated due to operator splitting. Consequently, for the GTO-Schwarz, the advection plays no role in computing the optimized Robin parameters. In addition, it was observed numerically that the GTP-Schur does not perform well when advection is dominant; particularly, the convergence speed with the (generalized) Neumann-Neumann preconditioner can be even slower than using no preconditioner.

The objective of this work is to develop fully implicit local time-stepping methods for heterogeneous linear transport problems based on global-in-time DD and the mixed *hybrid* finite element method proposed in [46, 13]. The finite element space is defined using the lowest-order Raviart-Thomas elements in which the total flux is the vector variable, and the Lagrange multiplier arising in the hybridization is used to discretize the advective term. Note that for the operator splitting scheme considered in [37], the flux variable approximates the diffusive flux only, and the advective term is approximated using an upwind operator based on the information from the adjacent elements. Differently from [37], here we will formulate the fully discrete interface problems for the GTP-Schur and GTO-Schwarz methods where there are no separate interface unknowns for the advection and diffusion. In addition, unlike [37] where the advection is treated explicitly and the diffusion implicitly, the methods proposed in this work are fully implicit with no CFL constraint on the time step size. For the GTO-Schwarz method, the Robin parameters are optimized by taking into account the effects of both advection and diffusion, and we shall prove the convergence of the associated discrete OSWR algorithm with nonconforming time grids. Note that in this work we focus on the use of local time stepping and only treat conforming spatial discretization. The reader is referred to [18, 3, 4, 10, 38], where mortar mixed methods on nonmatching spatial grids are developed.

The rest of the paper is organized as follows: in the next section we present the model problem and its spatial discretization by the upwind-mixed hybrid finite element method [46, 13]. In Section 3, we formulate two global-in-time decoupling methods using

3

the semi-discrete physical and Robin transmission conditions. The nonconforming time discretization and the fully discrete interface problems are introduced in Section 4; convergence of the OSWR algorithm is also proved where different time steps are used in the subdomains. In Section 5, two-dimensional numerical experiments are carried out to investigate the performance of the proposed methods on different test cases with various Peclét numbers, including one prototype for nuclear waste disposal simulation.

2. Model problem and its spatial discretization by mixed hybrid finite elements

For a bounded domain Ω of $\mathbb{R}^2$ with Lipschitz boundary $\partial\Omega$ and some fixed time $T > 0$, consider the following linear advection-diffusion problem

$$
\begin{aligned}
\omega\partial_t c + \nabla \cdot (\boldsymbol{u}c - \boldsymbol{D}\nabla c) &= f &&\text{in } \Omega \times (0,T), \\
c &= 0 &&\text{on } \partial\Omega \times (0,T), \\
c(\cdot,0) &= c_0 &&\text{in } \Omega,
\end{aligned}
\tag{2.1}
$$

where c is the concentration of a contaminant dissolved in a fluid, f the source term, ω the porosity, $\boldsymbol{u}$ the Darcy velocity (*assumed to be given and time independent*), $\boldsymbol{D}$ a symmetric time-independent diffusion tensor. For simplicity, we have imposed only Dirichlet boundary conditions; the analysis presented in the following can be generalized to other types of boundary conditions. Here and throughout the paper, we assume:

(A1) ω is bounded above and below by positive constants, $0 < \omega_- \leq \omega(\boldsymbol{x}) \leq \omega_+$ for all $\boldsymbol{x} \in \Omega$;

(A2) There exist positive constants δ_- and δ_+ such that $\delta_-|\boldsymbol{y}|^2 \leq \boldsymbol{y}^T\boldsymbol{D}^{-1}(\boldsymbol{x})\boldsymbol{y} \leq \delta_+|\boldsymbol{y}|^2$ for all $\boldsymbol{y} \in \mathbb{R}^2$ and $\boldsymbol{x} \in \Omega$;

(A3) $\boldsymbol{u} \in (W^{1,\infty}(\Omega))^2$, $f \in C(0,T;L^2(\Omega))$ and $c \in H_0^1(\Omega)$.

We rewrite (2.1) in an equivalent mixed form by introducing the vector field $\boldsymbol{\varphi}$, which consists of both diffusive and advective flux [46, 13]:

$$
\begin{aligned}
\omega\partial_t c + \nabla \cdot \boldsymbol{\varphi} &= f &&\text{in } \Omega \times (0,T), \\
\boldsymbol{\varphi} &= -\boldsymbol{D}\nabla c + \boldsymbol{u}c &&\text{in } \Omega \times (0,T),
\end{aligned}
\tag{2.2}
$$

together with the boundary and initial conditions as in (2.1).

We make use of standard notation for Sobolev spaces and their associated norms to define the weak formulations and perform convergence analysis in Section 4. In particular, we denote by $(\cdot,\cdot)$ the inner product on $L^2(\Omega)$ or $(L^2(\Omega))^2$, and by $\|\cdot\|_l$ the norm on $H^l(\Omega) = W^{l,2}(\Omega)$ (when $l = 0$, $H^l(\Omega)$ coincides with $L^2(\Omega)$). For a measurable subset $\Theta \subset \Omega$, we write $(\cdot,\cdot)_\Theta$ (respectively, $\langle\cdot,\cdot\rangle_{\partial\Theta}$) to indicate the inner product on Θ (respectively, $\partial\Theta$), and $\|\cdot\|_{l,\Theta}$ for the norms considered on Θ. The mixed variational formulation of (2.2) is given by:

4

For a.e. $t \in (0, T)$, find $(c(t), \boldsymbol{\varphi}(t)) \in L^2(\Omega) \times H(\text{div}, \Omega)$ such that

$$
\begin{aligned}
(\omega \partial_t c, \mu) + (\nabla \cdot \boldsymbol{\varphi}, \mu) &= (f, \mu), \quad \forall \mu \in L^2(\Omega), \\
(\boldsymbol{D}^{-1} \boldsymbol{\varphi}, \boldsymbol{v}) - (\boldsymbol{D}^{-1} \boldsymbol{u} c, \boldsymbol{v}) - (\nabla \cdot \boldsymbol{v}, c) &= 0, \qquad \forall \boldsymbol{v} \in H(\text{div}, \Omega).
\end{aligned}
\tag{2.3}
$$

Under the assumptions (A1) - (A3), there exists a unique solution $(c, \boldsymbol{\varphi}) \in H^1\left(0, T; L^2(\Omega)\right) \cap L^2(0, T; H^2(\Omega) \times L^2\left(0, T; H(\text{div}, \Omega)\right)$ to problem (2.3) as shown in [13, Theorem 3.2].

To find numerical solutions to (2.3), we use a mixed hybrid finite element (MHFE) method proposed in [46, 13]. Assume Ω is a rectangular domain and let $\mathcal{K}_h$ be a finite element partition of Ω into rectangles. Denote by $\mathcal{E}_h$ the set of all edges of elements of $\mathcal{K}_h$: $\mathcal{E}_h := \mathcal{E}_h^I \cup \mathcal{E}_h^D$, where $\mathcal{E}_h^I$ is the set of all interior edges and $\mathcal{E}_h^D$ the set of all edges on the boundary. For $K \in \mathcal{K}_h$, let $\boldsymbol{n}_K$ be the unit, normal, outward-pointing vector field on the boundary ∂K; for each edge $E \subset \partial K$, we denote by $\boldsymbol{n}_E$ the unit normal vector of E, outward to K. Let $h_K = \text{diam}(K)$ and $h = \max_{K \in \mathcal{K}_h} h_K$. The MHFE scheme is based on the mixed finite elements together with the hybridization technique, in which the continuity constraint of the normal components of the fluxes over inter-element edges is relaxed via the use of Lagrange multipliers. The discrete spaces for the scalar and vector variables are defined based on the lowest-order Raviart-Thomas space as

$$
\begin{aligned}
M_h &:= \left\{ \mu \in L^2(\Omega) : \mu_{|K} = \text{constant}, \ \forall K \in \mathcal{K}_h \right\}, \\
\Sigma_K &:= \left\{ \boldsymbol{v} : K \to \mathbb{R}^2, \ \boldsymbol{v} = \left(a_K + b_K x, a_K' + b_K' y \right), \ (a_K, b_K, a_K', b_K') \in \mathbb{R}^4 \right\}, \ \text{for } K \in \mathcal{K}_h, \\
\Sigma_h &:= \left\{ \boldsymbol{v} \in (L^2(\Omega))^2 : \boldsymbol{v}|_K \in \Sigma_K, \ \forall K \in \mathcal{K}_h \right\} \subset (L^2(\Omega))^2.
\end{aligned}
$$

The discrete space for the Lagrange multiplier representing the trace of the concentration on the edges is given by

$$
\Theta_h := \left\{ \theta \in L^2(\mathcal{E}_h) : \theta|_E = \text{ constant on E}, \ \forall E \in \mathcal{E}_h \text{ and } \theta|_E = 0, \ \forall E \in \mathcal{E}_h^D \right\}.
$$

For $c_h(t) \in M_h$, we have the unique representation

$$
c_h(t, \boldsymbol{x}) = \sum_{K \in \mathcal{K}_h} c_K(t) \psi_K(\boldsymbol{x}),
$$

where ψ_K is the characteristic function of element $K \in \mathcal{K}_h$, and c_K represents the average value of c_h on K. Similarly, for $\theta_h \in \Theta_h$, it can be expressed as

$$
\theta_h(t, \xi) = \sum_{E \in \mathcal{E}_h} \theta_E(t) \psi_E(\xi),
$$

where ψ_E is the characteristic function of edge $E \in \mathcal{E}_h$, and θ_E is the average values of θ_h on E. For $\boldsymbol{\varphi}_h \in \Sigma_h$, the function is defined locally as

$$
\boldsymbol{\varphi}_h(t, \boldsymbol{x})|_K = \sum_{E \subset \partial K} \varphi_{KE}(t) \boldsymbol{w}_{KE}(\boldsymbol{x}),
$$

5

where φ_{KE} is the normal flux leaving K through the edge E and $\{\boldsymbol{w}_{KE}\}_{E \subset \partial K}$ are the basis functions of the local Raviart-Thomas space Σ_K satisfying

$$\int_{E'} \boldsymbol{w}_{KE} \cdot \boldsymbol{n}_K = \delta_{E,E'}, \ \forall E' \subset \partial K.$$

We denote by $\boldsymbol{u}_h$ the projection of $\boldsymbol{u}$ on Σ_h which is defined as

$$\boldsymbol{u}_h := \sum_{K \in \mathcal{K}_h} \sum_{E \subset \partial K} u_{KE} \boldsymbol{w}_{KE}(\boldsymbol{x}), \tag{2.4}$$

where $u_{KE} = \frac{1}{|E|} \int_E \boldsymbol{u} \cdot \boldsymbol{n}_K$, $\forall E \subset \partial K$, $\forall K \in \mathcal{K}_h$. The mixed hybrid variational formulation for the monodomain problem is given by:

For a.e. $t \in (0, T)$, find $(c_h(t), \boldsymbol{\varphi}_h(t), \theta_h(t)) \in M_h \times \Sigma_h \times \Theta_h$ such that

$$\begin{aligned}
(\omega \partial_t c_h, \mu_h) + (\nabla \cdot \boldsymbol{\varphi}_h, \mu_h) &= (f, \mu_h), \ \forall \mu_h \in M_h, \\
\left(\boldsymbol{D}^{-1} \boldsymbol{\varphi}_h, \boldsymbol{v}_h\right) - \left(\boldsymbol{D}^{-1} \boldsymbol{u}_h c_h, \boldsymbol{v}_h\right) - (\nabla \cdot \boldsymbol{v}_h, c_h) + \sum_{K \in \mathcal{K}_h} \langle \theta_h, \boldsymbol{v}_h \cdot \boldsymbol{n}_K \rangle_{\partial K} &= 0, \quad \forall \boldsymbol{v}_h \in \Sigma_h, \\
\sum_{K \in \mathcal{K}_h} \langle \vartheta_h, \boldsymbol{\varphi}_h \cdot \boldsymbol{n}_K \rangle_{\partial K} &= 0, \quad \forall \vartheta \in \Theta_h.
\end{aligned} \tag{2.5}$$

The last equation enforces the continuity of the normal components of the fluxes over inter-element edges so that the vector variable $\boldsymbol{\varphi}_h \in \Sigma_h$ belongs to $H(\mathrm{div}, \Omega)$.

For the space-discrete advection term in $(2.5)_2$, instead of using the piecewise constant concentration, we employ the Lagrange multiplier as in [46, 13] and utilize (2.4) to obtain the following upwind-mixed scheme:

$$\begin{aligned}
(\omega \partial_t c_h, \mu_h) + (\nabla \cdot \boldsymbol{\varphi}_h, \mu_h) &= (f, \mu_h), \quad \forall \mu_h \in M_h, \\
\left(\boldsymbol{D}^{-1} \boldsymbol{\varphi}_h, \boldsymbol{v}_h\right) - \sum_{K \in \mathcal{K}_h} \sum_{E \subset \partial K} u_{KE} \, \mathcal{U}_{KE}\left(c_K, \theta_E\right) \left(\boldsymbol{D}^{-1} \boldsymbol{w}_{KE}, \boldsymbol{v}_h\right) & \\
- (\nabla \cdot \boldsymbol{v}_h, c_h) + \sum_{K \in \mathcal{K}_h} \langle \theta_h, \boldsymbol{v}_h \cdot \boldsymbol{n}_K \rangle_{\partial K} &= 0, \quad \forall \boldsymbol{v}_h \in \Sigma_h, \\
\sum_{K \in \mathcal{K}_h} \langle \vartheta_h, \boldsymbol{\varphi}_h \cdot \boldsymbol{n}_K \rangle_{\partial K} &= 0, \quad \forall \vartheta \in \Theta_h,
\end{aligned} \tag{2.6}$$

where the upwind values $\mathcal{U}_{KE}\left(c_K, \theta_E\right)$ are computed by

$$\mathcal{U}_{KE}\left(c_K, \theta_E\right) = \begin{cases} c_K, & \text{if } u_{KE} \geq 0, \\ 2\theta_E - c_K, & \text{otherwise.} \end{cases} \tag{2.7}$$

We can also replace the upwind values by the Lagrange multipliers:

$$\mathcal{U}_{KE}\left(c_K, \theta_E\right) = \theta_E. \tag{2.8}$$

Numerical tests [46] suggest that the scheme (2.6) with the upwind values defined by (2.7) is efficient for strongly advection-dominated problems, while using (2.8) gives good performance for the case where advection is moderately dominant. Both choices preserve the convergence properties of the discretization scheme, and we shall consider formula (2.8) in our numerical experiments. By taking the test functions to be basis functions in (2.6), we obtain a system of linear equations for mass conservation, the flux and its continuity over internal edges.

(i) Mass conservation equation. Let ω_K be the average of ω on K, $(2.6)_1$ implies

$$|K|\omega_K \partial_t c_K + \sum_{E \subset \partial K} \varphi_{KE} = \int_K f \, d\boldsymbol{x}, \quad \forall K \in \mathcal{K}_h. \tag{2.9}$$

(ii) Equation for the flux. Denote by $A_{KEE'} = \int_K (\boldsymbol{D}^{-1} \boldsymbol{w}_{KE'}) \cdot \boldsymbol{w}_{KE} \, d\boldsymbol{x}$, for $E, E' \subset \partial K$, $K \in \mathcal{K}_h$, $(2.6)_2$ becomes

$$\sum_{E' \subset \partial K} A_{KEE'} \varphi_{KE'} - \sum_{E' \subset \partial K} A_{KEE'} u_{KE'} \, \mathcal{U}_{KE'} (c_K, \theta_{E'}) - c_K + \theta_E = 0, \quad \forall K \in \mathcal{K}_h, \forall E \subset \partial K. \tag{2.10}$$

(iii) Continuity of the flux over internal edges. It is deduced from $(2.6)_3$ that

$$\sum_{\substack{K \in \mathcal{K}_h \\ E \subset \partial K}} \varphi_{KE} = 0, \quad \forall E \in \mathcal{E}_h^I. \tag{2.11}$$

The system (2.9)-(2.11) is completed with some appropriate boundary conditions and initial condition.

Remark 2.1. *The fully discrete problem obtained by discretizing* (2.6) *in time using the implicit Euler method was analyzed in [13, Theorem 4.4]. Expected error estimates were proved, given that the choice of upwind values satisfies the following inequality*

$$|\mathcal{U}_{KE} (c_K, \lambda_E) - c_K| \le C|\lambda_E - c_K|, \quad \forall E \subset \partial K, \forall K \in \mathcal{K}_h,$$

for some constant C independent of the mesh size and time step size. Note that the upwind values given by either (2.7) *or* (2.8) *satisfy this requirement.*

3. Semi-discrete, global-in-time domain decomposition methods

We use nonoverlapping domain decomposition methods that allow different time steps to solve the semi-discrete problem (2.5). For simplicity, we consider a decomposition of Ω into two nonoverlapping subdomains Ω_1 and Ω_2 separated by an interface Γ:

$$\Omega_1 \cap \Omega_2 = \emptyset; \quad \Gamma = \partial \Omega_1 \cap \partial \Omega_2 \cap \Omega, \quad \Omega = \Omega_1 \cup \Omega_2 \cup \Gamma.$$

7

The analysis can be generalized to the case of multiple subdomains (see Section 5). We assume that the partitions $\mathcal{K}_{h,1}$ of subdomain Ω_1 and $\mathcal{K}_{h,2}$ of subdomain Ω_2 are such that their union $\mathcal{K}_h = \cup_{i=1}^2 \mathcal{K}_{h,i}$ forms a finite element partition of Ω. Let $\mathcal{E}_{h,i}$ be the set of all edges of elements of $\mathcal{K}_{h,i}$ and $\mathcal{E}_{h,i}^D$ the set of edges on the external boundary $\partial\Omega_i \cap \partial\Omega$, for $i = 1, 2$. Notice that in this work we focus on the use of different time steps, and assume the spatial discretization is conforming. Thus we denote by $\mathcal{E}_h^\Gamma$ the set of edges of elements of $\mathcal{K}_{h,1}$ or $\mathcal{K}_{h,2}$ that lie on Γ. For $i = 1, 2$, let $\boldsymbol{n}_i$ denote the unit, normal, outward-pointing vector field on $\partial\Omega_i$, and for any scalar, vector or tensor-valued function ψ defined on Ω, let ψ_i denote the restriction of ψ to Ω_i.

Let M_h, Σ_h and Θ_h denote the mixed finite element spaces and the Lagrange multiplier space as defined in Section 2, and let $M_{h,i}$, $\Sigma_{h,i}$ and $\Theta_{h,i}$, $i = 1, 2$, be the spaces of restrictions of the functions in these spaces to Ω_i. In particular:

$$\Theta_{h,i} := \left\{ \theta \in L^2(\mathcal{E}_{h,i}) : \theta|_E = \text{ constant on E}, \ \forall E \in \mathcal{E}_{h,i} \text{ and } \theta|_E = 0, \ \forall E \in \mathcal{E}_{h,i}^D \right\}.$$

In addition, we define the space

$$\Theta_{h,i}^{\Gamma,0} := \left\{ \theta \in \Theta_{h,i} : \theta|_E = 0, \ \forall E \in \mathcal{E}_h^\Gamma \right\},$$

to take into account the interface as part of the subdomain boundary. As for the single domain case, we have the following representations of functions in the subdomain finite element spaces:

$$
\begin{aligned}
c_{h,i}(t, \boldsymbol{x}) &= \sum_{K \in \mathcal{K}_{h,i}} c_{i,K}(t)\psi_K(\boldsymbol{x}), \quad \theta_{h,i}(t, \xi) = \sum_{E \in \mathcal{E}_{h,i}} \theta_{i,E}(t)\psi_E(\xi), \\
\boldsymbol{\varphi}_{h,i}(t, \boldsymbol{x}) &= \sum_{K \in \mathcal{K}_{h,i}} \sum_{E \subset \partial K} \varphi_{i,KE}(t)\boldsymbol{w}_{KE}(\boldsymbol{x}).
\end{aligned}
\tag{3.1}
$$

Consequently, we may identify functions $c_{h,i} \in M_{h,i}$ with vectors $(c_{i,K})_{K \in \mathcal{K}_{h,i}}$, $\theta_{h,i} \in \Theta_{h,i}$ with $(\theta_{i,E})_{E \in \mathcal{E}_{h,i}}$, and $\boldsymbol{\varphi}_{h,i} \in \Sigma_{h,i}$ with $(\varphi_{i,KE})_{K \in \mathcal{K}_{h,i}, E \subset K}$ when necessary to simplify the presentation. To define the transmission conditions between the subdomains, we introduce the following interface space consisting of piecewise constant functions on Γ:

$$\Lambda_h = \left\{ \lambda \in L^2(\mathcal{E}_h^\Gamma) : \lambda|_E = \text{ constant on E}, \ \forall E \in \mathcal{E}_h^\Gamma \right\}. \tag{3.2}$$

With the notation introduced above, the monodomain problem (2.5) is equivalent to the following time-dependent subdomain problems in Ω_1 and Ω_2:

$$
\begin{aligned}
& (\omega_i \partial_t c_{h,i}, \mu_h)_{\Omega_i} + (\nabla \cdot \boldsymbol{\varphi}_{h,i}, \mu_h)_{\Omega_i} = (f, \mu_h)_{\Omega_i}, \quad \forall \mu_h \in M_{h,i}, \\
& \left(\boldsymbol{D}_i^{-1}\boldsymbol{\varphi}_{h,i}, \boldsymbol{v}_h\right)_{\Omega_i} - \sum_{K \in \mathcal{K}_{h,i}} \sum_{E \subset \partial K} u_{i,KE}\, \mathcal{U}_{KE}\left(c_{i,K}, \theta_{i,E}\right)\left(\boldsymbol{D}_i^{-1}\boldsymbol{w}_{KE}, \boldsymbol{v}_h\right)_{\Omega_i} \\
& \hspace{2cm} - (\nabla \cdot \boldsymbol{v}_h, c_{h,i})_{\Omega_i} + \sum_{K \in \mathcal{K}_{h,i}} \langle \theta_{h,i}, \boldsymbol{v}_h \cdot \boldsymbol{n}_K \rangle_{\partial K} = 0, \ \forall \boldsymbol{v}_h \in \Sigma_{h,i}, \\
& \sum_{K \in \mathcal{K}_h} \langle \vartheta_h, \boldsymbol{\varphi}_{h,i} \cdot \boldsymbol{n}_K \rangle_{\partial K} = 0, \quad \forall \vartheta_h \in \Theta_{h,i}^{\Gamma,0},
\end{aligned}
\tag{3.3}
$$

8

for $i = 1, 2$, together with the time-dependent transmission conditions:

$$\begin{aligned} \langle \theta_{h,1}(t), \eta_h \rangle_\Gamma &= \langle \theta_{h,2}(t), \eta_h \rangle_\Gamma, \\ \langle \eta_h, \boldsymbol{\varphi}_{h,1}(t) \cdot \boldsymbol{n}_1 + \boldsymbol{\varphi}_{h,2}(t) \cdot \boldsymbol{n}_2 \rangle_\Gamma &= 0, \end{aligned} \qquad \forall \eta_h \in \Lambda_h, \tag{3.4}$$

for $t \in (0, T)$, where $\langle \cdot, \cdot \rangle_\Gamma$ denotes the inner product of $L^2(\Gamma)$. Alternatively, one may use the following equivalent Robin transmission conditions:

$$\begin{aligned} \langle -\boldsymbol{\varphi}_{h,1}(t) \cdot \boldsymbol{n}_1 + \alpha_{1,2}\theta_{h,1}(t), \eta_h \rangle_\Gamma &= \langle -\boldsymbol{\varphi}_{h,2}(t) \cdot \boldsymbol{n}_1 + \alpha_{1,2}\theta_{h,2}(t), \eta_h \rangle_\Gamma, \\ \langle -\boldsymbol{\varphi}_{h,2}(t) \cdot \boldsymbol{n}_2 + \alpha_{2,1}\theta_{h,2}(t), \eta_h \rangle_\Gamma &= \langle -\boldsymbol{\varphi}_{h,1}(t) \cdot \boldsymbol{n}_2 + \alpha_{2,1}\theta_{h,1}(t), \eta_h \rangle_\Gamma, \end{aligned} \qquad \forall \eta_h \in \Lambda_h, \tag{3.5}$$

where $\alpha_{1,2}$ and $\alpha_{2,1}$ are a pair of positive parameters. By the definition of the finite dimensional approximation spaces, the transmission condition in (3.4) can be rewritten as

$$\begin{aligned} \theta_{1,E}(t) &= \theta_{2,E}(t), \\ \varphi_{1,KE}(t) + \varphi_{2,K'E}(t) &= 0, \end{aligned} \qquad \forall\, E \in \mathcal{E}_h^\Gamma,\ t \in (0, T), \tag{3.6}$$

where $E = \partial K \cap \partial K'$, with $K \in \mathcal{K}_{h,1}$ and $K' \in \mathcal{K}_{h,2}$ (i.e. K and K' are elements in different subdomains sharing the interface edge E). Similarly, the Robin transmission conditions (3.5) are equivalent to

$$\begin{aligned} -\varphi_{1,KE}(t) + \alpha_{1,2}\theta_{1,E}(t) &= \varphi_{2,K'E}(t) + \alpha_{1,2}\theta_{2,E}(t) \\ -\varphi_{2,K'E}(t) + \alpha_{2,1}\theta_{2,E}(t) &= \varphi_{1,KE}(t) + \alpha_{2,1}\theta_{1,E}(t) \end{aligned} \qquad \forall E \in \mathcal{E}_h^\Gamma,\ t \in (0, T). \tag{3.7}$$

The first method that we consider is based on (3.3) together with the physical transmission conditions (3.6) while the second method is based on (3.3) together with the Robin transmission conditions (3.7). For the latter method, the parameters $\alpha_{i,j}$ may be optimized to improve the convergence rate of the iterative scheme. For precise details of how the optimization is carried out, see [23, 32].

3.1. Method 1: Global-in-Time Preconditioned Schur (GTP-Schur)

We impose the first transmission condition in (3.4) as Dirichlet boundary conditions on the interface of the subdomain problems:

$$\theta_{h,i}(t)|_\Gamma = \lambda_h(t), \quad t \in (0, T), \text{ for } i = 1, 2, \tag{3.8}$$

for some given $\lambda_h(t) \in \Lambda_h$. We introduce the space

$$\Theta_{h,i}^{\Gamma,\lambda_h} := \big\{ \theta \in L^2(\mathcal{E}_{h,i}) : \theta|_E = \text{ constant on E, } \forall E \in \mathcal{E}_{h,i}, \theta|_E = 0, \ \forall E \in \mathcal{E}_{h,i}^D,$$
$$\text{and } \theta|_E = \lambda_h|_E, \ \forall E \in \mathcal{E}_{h,i}^\Gamma \big\}, \tag{3.9}$$

for the Lagrange multipliers with nonhomogeneous Dirichlet conditions on the interface Γ. For $i = 1, 2$, we denote by

$$(c_{h,i}(\lambda_h, f, c_0), \boldsymbol{\varphi}_{h,i}(\lambda_h, f, c_0), \theta_{h,i}(\lambda_h, f, c_0)) \in H^1(0, T; M_{h,i}) \times L^2(0, T; \Sigma_{h,i}) \times L^2(0, T; \Theta_{h,i}^{\Gamma,\lambda_h})$$

9

the solution to the time-dependent subdomain problem with Dirichlet interface condition (3.8):

$$(\omega_i \partial_t c_{h,i}, \mu_h)_{\Omega_i} + (\nabla \cdot \boldsymbol{\varphi}_{h,i}, \mu_h)_{\Omega_i} = (f, \mu_h)_{\Omega_i}, \quad \forall \mu_h \in M_{h,i},$$

$$\left(\boldsymbol{D}_i^{-1}\boldsymbol{\varphi}_{h,i}, \boldsymbol{v}_h\right)_{\Omega_i} - \sum_{K \in \mathcal{K}_{h,i}} \sum_{E \subset \partial K} u_{i,KE} \, \mathcal{U}_{KE}\left(c_{i,K}, \theta_{i,E}\right) \left(\boldsymbol{D}_i^{-1}\boldsymbol{w}_{KE}, \boldsymbol{v}_h\right)_{\Omega_i}$$

$$- (\nabla \cdot \boldsymbol{v}_h, c_{h,i})_{\Omega_i} + \sum_{K \in \mathcal{K}_{h,i}} \langle \theta_{h,i}, \boldsymbol{v}_h \cdot \boldsymbol{n}_K \rangle_{\partial K} = 0, \quad \forall \boldsymbol{v}_h \in \Sigma_{h,i}, \qquad (3.10)$$

$$\sum_{K \in \mathcal{K}_h} \langle \vartheta_h, \boldsymbol{\varphi}_{h,i} \cdot \boldsymbol{n}_K \rangle_{\partial K} = 0, \quad \forall \vartheta_h \in \Theta_{h,i}^{\Gamma,0},$$

$$(c_{h,i}(0), \mu_h)_{\Omega_i} = (c_0, \mu_h)_{\Omega_i}, \quad \forall \mu_h \in M_{h,i}.$$

The semi-discrete interface problem for Method 1 is obtained by enforcing the remaining transmission condition, i.e. the flux continuity equation. Toward that end, we define the interface operators, for $i = 1, 2$:

$$\mathcal{S}_{h,i} : \quad L^2(0, T; \Lambda_h) \quad \longrightarrow \quad L^2(0, T; \Lambda_h),$$
$$\lambda_h \quad \mapsto \quad -\boldsymbol{\varphi}_{h,i}(\lambda_h, 0, 0) \cdot \boldsymbol{n}_i|_\Gamma,$$

and

$$\chi_{h,i} : \quad L^2(0, T; \Omega_i) \times H_*^1(\Omega_i) \quad \longrightarrow \quad L^2(0, T; \Lambda_h),$$
$$(f, c_0) \quad \mapsto \quad \boldsymbol{\varphi}_{h,i}(0, f, c_0) \cdot \boldsymbol{n}_i|_\Gamma,$$

where $H_*^1(\Omega_i) = \{\mu \in H^1(\Omega_i) : v = 0 \text{ on } \partial\Omega_i \cap \partial\Omega\}$. The operators $\mathcal{S}_{h,i}$, $i = 1, 2$, are the (time-dependent) Schur operators. Letting $\mathcal{S}_h = \mathcal{S}_{h,1} + \mathcal{S}_{h,2}$ and $\chi_h = \chi_{h,1} + \chi_{h,2}$, we rewrite problem (3.3)-(3.4) as a space-time interface problem:

Find $\lambda_h \in L^2(0, T; \Lambda_h)$, such that

$$\int_0^T \int_\Gamma (\mathcal{S}_h \lambda_h) \, \eta_h \, d\gamma \, dt = \int_0^T \int_\Gamma \chi_h \, \eta_h \, d\gamma \, dt, \quad \forall \eta_h \in L^2(0, T; \Lambda_h). \qquad (3.11)$$

The interface problem (3.11) is solved iteratively, and to enhance the convergence of the iteration, we apply a Neumann-Neumann type preconditioner similarly to the one proposed for the pure diffusion case [34]. For a function $\phi_h \in L^2(0, T; \Lambda_h)$, we define the following spaces to handle Neumann boundary conditions involved in the preconditioner:

$$\Sigma_{h,i}^{\Gamma,\phi_h} = \left\{ \boldsymbol{v} \in \Sigma_{h,i} : v_{KE} = \phi_h|_E, \quad \forall E \in \mathcal{E}_h^\Gamma, \, K \in \mathcal{K}_{h,i} \text{ such that } E \subset \partial K \right\},$$

$$\Sigma_{h,i}^{\Gamma,0} = \left\{ \boldsymbol{v} \in \Sigma_{h,i} : v_{KE} = 0, \quad \forall E \in \mathcal{E}_h^\Gamma, \, K \in \mathcal{K}_{h,i} \text{ such that } E \subset \partial K \right\}.$$

The Neumann-Neumann preconditioner for (3.11) is given by:

$$(\sigma_{1,2}\mathcal{N}_{h,1} + \sigma_{2,1}\mathcal{N}_{h,2})\mathcal{S}_h \lambda_h = \widetilde{\chi_h}, \qquad (3.12)$$

10

where $\sigma_{i,j}$ are some weights such that $\sigma_{1,2}+\sigma_{2,1}=1$, and $\mathcal{N}_{h,i}$ is a (pseudo-)inverse operator of $\mathcal{S}_{h,i}$ defined, for $\phi_h \in L^2(0,T;\Lambda_h)$, as

$$\mathcal{N}_{h,i}\psi_h = \theta_{h,i}(\phi_h)|_\Gamma, \quad i=1,2, \tag{3.13}$$

where $(c_{h,i}(\phi_h), \boldsymbol{\varphi}_{h,i}(\phi_h), \theta_{h,i}(\phi_h)) \in H^1(0,T;M_{h,i}) \times L^2(0,T;\Sigma_{h,i}^{\Gamma,\phi_h}) \times L^2(0,T;\Theta_{h,i})$, $i = 1, 2$, is the solution to the time-dependent subdomain problem with Neumann boundary conditions on the interface and zero initial condition:

$$(\omega_i \partial_t c_{h,i}, \mu_h)_{\Omega_i} + (\nabla \cdot \boldsymbol{\varphi}_{h,i}, \mu_h)_{\Omega_i} = 0, \quad \forall \mu_h \in M_{h,i},$$

$$\left(\boldsymbol{D}_i^{-1}\boldsymbol{\varphi}_{h,i}, \boldsymbol{v}_h\right)_{\Omega_i} - \sum_{K \in \mathcal{K}_{h,i}} \sum_{E \subset \partial K} u_{i,KE} \, \mathcal{U}_{KE}\left(c_{i,K}, \theta_{i,E}\right) \left(\boldsymbol{D}_i^{-1}\boldsymbol{w}_{KE}, \boldsymbol{v}_h\right)_{\Omega_i}$$

$$- (\nabla \cdot \boldsymbol{v}_h, c_{h,i})_{\Omega_i} + \sum_{K \in \mathcal{K}_{h,i}} \langle \theta_{h,i}, \boldsymbol{v}_h \cdot \boldsymbol{n}_K \rangle_{\partial K} = 0, \quad \forall \boldsymbol{v}_h \in \Sigma_{h,i}^{\Gamma,0}, \tag{3.14}$$

$$\sum_{K \in \mathcal{K}_h} \langle \vartheta_h, \boldsymbol{\varphi}_h \cdot \boldsymbol{n}_K \rangle_{\partial K} = 0, \quad \forall \vartheta_h \in \Theta_{h,i}^{\Gamma,0}.$$

Remark 3.1. *Convergence analysis of the GMRES algorithm for the interface problem (3.11) is challenging, even for the pure diffusion problem [34], as the Steklov-Poincaré (or Schur) operator is a nonsymmetric space-time interface operator. Recently, a space-time multiscale mortar mixed finite element method for parabolic equations has been developed in [38] where both nonmatching spatial grids and nonconforming time grids are used in the subdomains. Under suitable assumptions on the spatial and temporal mortar grids, GMRES applied to the fully discrete interface problem of the GT-Schur method (with no preconditioner) is shown to converge via the use of the field-of-values estimates. In this work, we aim to first investigate numerically the convergence of the GT-Schur method and the performance of the Neumann-Neumann preconditioner for problems with discontinuous coefficients and various Peclét numbers as presented in Section 5. The analysis of GMRES convergence and the preconditioner for the GT-Schur method to solve the advection-diffusion equation shall be studied separately in future work.*

3.2. Method 2: Global-in-Time Optimized Schwarz (GTO-Schwarz)

We impose Robin transmission conditions (3.7) as boundary conditions on $\Gamma \times (0,T)$ for solving the subdomain problems:

$$(-\boldsymbol{\varphi}_{h,i}(t) \cdot \boldsymbol{n}_i + \alpha_{i,j}\theta_{h,i}(t))\,|_\Gamma = \zeta_{h,i}(t), \quad t \in (0,T), \tag{3.15}$$

for given $\zeta_{h,i} \in L^2(0,T;\Lambda_h)$ and for $i=1,2$. Denote by

$$(c_{h,i}(\zeta_{h,i}, f, c_0), \boldsymbol{\varphi}_{h,i}(\zeta_{h,i}, f, c_0), \theta_{h,i}(\zeta_{h,i}, f, c_0)) \in H^1(0,T;M_{h,i}) \times L^2(0,T;\Sigma_{h,i}) \times L^2(0,T;\Theta_{h,i})$$

the solution to the time-dependent subdomain problem with Robin interface condition (3.15):

$$(\omega_i \partial_t c_{h,i}, \mu_h)_{\Omega_i} + (\nabla \cdot \boldsymbol{\varphi}_{h,i}, \mu_h)_{\Omega_i} = (f, \mu_h)_{\Omega_i}, \ \forall \mu_h \in M_{h,i},$$

$$\left(\boldsymbol{D}_i^{-1} \boldsymbol{\varphi}_{h,i}, \boldsymbol{v}_h\right)_{\Omega_i} - \sum_{K \in \mathcal{K}_{h,i}} \sum_{E \subset \partial K} u_{i,KE} \, \mathcal{U}_{KE}\left(c_{i,K}, \theta_{i,E}\right) \left(\boldsymbol{D}_i^{-1} \boldsymbol{w}_{KE}, \boldsymbol{v}_h\right)_{\Omega_i}$$

$$- (\nabla \cdot \boldsymbol{v}_h, c_{h,i})_{\Omega_i} + \sum_{K \in \mathcal{K}_h} \langle \theta_{h,i}, \boldsymbol{v}_h \cdot \boldsymbol{n}_K \rangle_{\partial K} = 0, \quad \forall \boldsymbol{v}_h \in \Sigma_{h,i},$$

$$\sum_{K \in \mathcal{K}_h} \langle \vartheta_h, \boldsymbol{\varphi}_{h,i} \cdot \boldsymbol{n}_K \rangle_{\partial K} = 0, \ \forall \vartheta_h \in \Theta_h^{\Gamma,0},$$

$$\langle -\boldsymbol{\varphi}_{h,i} \cdot \boldsymbol{n}_i + \alpha_{i,j} \theta_{h,i}, \eta_h \rangle_\Gamma = \langle \zeta_{h,i}, \eta_h \rangle_\Gamma, \quad \forall \eta_h \in \Lambda_h,$$

$$(c_{h,i}(0), \mu_h)_{\Omega_i} = (c_0, \mu_h)_{\Omega_i}, \quad \forall \mu_h \in M_{h,i}.$$

(3.16)

We define the interface operators:

$$\mathcal{S}_h^R : \ \left(L^2(0,T;\Lambda_h)\right)^2 \ \longrightarrow \ \left(L^2(0,T;\Lambda_h)\right)^2,$$

$$\begin{pmatrix} \zeta_{h,1} \\ \zeta_{h,2} \end{pmatrix} \ \mapsto \ \begin{pmatrix} \zeta_{h,1} - \left(-\boldsymbol{\varphi}_{h,2}(\zeta_{h,2},0,0) \cdot \boldsymbol{n}_1 + \alpha_{1,2}\theta_{h,2}(\zeta_{h,2},0,0)\right)|_\Gamma \\ \zeta_{h,2} - \left(-\boldsymbol{\varphi}_{h,1}(\zeta_{h,1},0,0) \cdot \boldsymbol{n}_2 + \alpha_{2,1}\theta_{h,1}(\zeta_{h,1},0,0)\right)|_\Gamma \end{pmatrix},$$

and

$$\chi_h^R : \ L^2(0,T;\Omega_i) \times H_*^1(\Omega_i) \ \longrightarrow \ \left(L^2(0,T;\Lambda_h)\right)^2,$$

$$(f, c_0) \ \mapsto \ \begin{pmatrix} \left(-\boldsymbol{\varphi}_{h,2}(0,f,c_0) \cdot \boldsymbol{n}_1 + \alpha_{1,2}\theta_{h,2}(0,f,c_0)\right)|_\Gamma \\ \left(-\boldsymbol{\varphi}_{h,1}(0,f,c_0) \cdot \boldsymbol{n}_2 + \alpha_{2,1}\theta_{h,1}(0,f,c_0)\right)|_\Gamma \end{pmatrix},$$

for $i = 1, 2$. The semi-discrete interface problem for Method 2 is given by:
    Find $(\zeta_{h,1}, \zeta_{h,2}) \in \left(H^1(0,T;\Lambda_h)\right)^2$ such that

$$\int_0^T \int_\Gamma \mathcal{S}_h^R \begin{pmatrix} \zeta_{h,1} \\ \zeta_{h,2} \end{pmatrix} \cdot \begin{pmatrix} \eta_{h,1} \\ \eta_{h,2} \end{pmatrix} d\gamma \, dt = \int_0^T \int_\Gamma \chi_h^R \cdot \begin{pmatrix} \eta_{h,1} \\ \eta_{h,2} \end{pmatrix} d\gamma \, dt, \ \forall (\eta_{h,1}, \eta_{h,2}) \in \left(L^2(0,T;\Lambda_h)\right)^2.$$

(3.17)

As for GTP-Schur, we solve the interface problem (3.17) iteratively using Jacobi iteration or GMRES. The former choice is equivalent to the *Optimized Schwarz waveform relaxation (OSWR) algorithm*: at the kth iteration, solve in parallel the subdomain problems:

$$\left(\omega_i \partial_t c_{h,i}^k, \mu_h\right)_{\Omega_i} + \left(\nabla \cdot \boldsymbol{\varphi}_{h,i}^k, \mu_h\right)_{\Omega_i} = (f, \mu_h)_{\Omega_i}, \ \forall \mu_h \in M_{h,i}$$

$$\left(\boldsymbol{D}_i^{-1} \boldsymbol{\varphi}_{h,i}^k, \boldsymbol{v}_h\right)_{\Omega_i} - \sum_{K \in \mathcal{K}_{h,i}} \sum_{E \subset \partial K} u_{i,KE} \, \mathcal{U}_{KE}\left(c_{i,K}^k, \theta_{i,E}^k\right) \left(\boldsymbol{D}_i^{-1} \boldsymbol{w}_{KE}, \boldsymbol{v}_h\right)_{\Omega_i}$$

$$- \left(\nabla \cdot \boldsymbol{v}_h, c_{h,i}^k\right)_{\Omega_i} + \sum_{K \in \mathcal{K}_h} \left\langle \theta_{h,i}^k, \boldsymbol{v}_h \cdot \boldsymbol{n}_K \right\rangle_{\partial K} = 0, \quad \forall \boldsymbol{v}_h \in \Sigma_{h,i},$$

$$\sum_{K \in \mathcal{K}_h} \left\langle \vartheta_h, \boldsymbol{\varphi}_{h,i}^k \cdot \boldsymbol{n}_K \right\rangle_{\partial K} = 0, \ \forall \vartheta_h \in \Theta_h^{\Gamma,0},$$

$$\left\langle -\boldsymbol{\varphi}_{h,i}^k \cdot \boldsymbol{n}_i + \alpha_{i,j} \theta_{h,i}^k, \eta_h \right\rangle_\Gamma = \left\langle -\boldsymbol{\varphi}_{h,j}^{k-1} \cdot \boldsymbol{n}_i + \alpha_{i,j} \theta_{h,j}^{k-1}, \eta_h \right\rangle_\Gamma, \quad \forall \eta_h \in \Lambda_h,$$

$$(c_{h,i}^k(0), \mu_h)_{\Omega_i} = (c_0, \mu_h)_{\Omega_i}, \quad \forall \mu_h \in M_{h,i}.$$

(3.18)

12

for $i = 1, 2$, with given initial guesses: $g_{i,j}(t) := -\varphi_{h,j}^0 \cdot \boldsymbol{n}_i + \alpha_{i,j}\theta_{h,j}^0 \in \Lambda_h$ for $i = 1, 2$, $j = 3 - i$ to start the first iterate. We will prove the convergence of the fully discrete OSWR algorithm with different subdomain time steps in the next section.

Remark 3.2. *The theoretical asymptotic behavior of optimized Robin parameters with Jacobi iteration was analyzed in [21, 6] for the linear advection-diffusion problems with constant coefficients, where the spatial domain is either the real line $\Omega = \mathbb{R}$ or the whole plane $\Omega = \mathbb{R}^2$. In particular, the convergence factor of OSWR with optimized Robin parameters and nonoverlapping subdomains behaves like $1 - O(h^{1/2})$.*

4. Nonconforming time discretizations

The GTP-Schur and GTO-Schwarz methods involve solving the subdomain problems globally in time, thus independent time discretizations can be used in the subdomains. We consider fully discrete problems with nonconforming time grids. Let $\mathcal{T}_1$ and $\mathcal{T}_2$ be two possibly different partitions of the time interval $(0, T)$ into sub-intervals (see Figure 1). We denote by $J_{i,m}$ the time interval $(t_{i,m}, t_{i,m-1}]$ and by $\Delta t_{i,m} := (t_{i,m} - t_{i,m-1})$ for $m = 1, \ldots, M_i$ and $i = 1, 2$, where for simplicity of exposition we have again supposed that we have only two subdomains. We use the the backward Euler method for discretizing in time, the same idea can be generalized to higher order methods. We denote by $P_0(\mathcal{T}_i, W)$
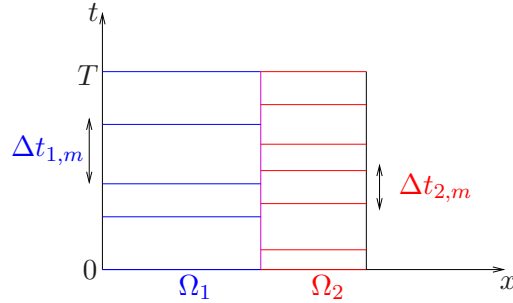

Figure 1: Nonconforming time grids in the subdomains.

the space of piecewise constant functions in time on grid $\mathcal{T}_i$ with values in W:

$$P_0(\mathcal{T}_i, W) = \{\psi : (0, T) \to W, \ \psi \text{ is constant on } J_{i,m}, \ \forall m = 1, \ldots, M_i\}. \qquad (4.1)$$

In order to exchange data on the space-time interface between different time grids, we define the following L^2 projection Π_{ji} from $P_0(\mathcal{T}_i, W)$ onto $P_0(\mathcal{T}_j, W)$ (see [24, 32]): for $\psi \in P_0(\mathcal{T}_i, W)$, $\Pi_{ji}\psi|_{J_{j,m}}$ is the average value of ψ on $J_{j,m}$, for $m = 1, \ldots, M_j$:

$$\Pi_{ji}(\psi)|_{J_{j,m}} = \frac{1}{|J_{j,m}|} \sum_{l=1}^{M_i} \int_{J_{j,m} \cap J_{i,l}} \psi. \qquad (4.2)$$

We use the algorithm described in [24] to effectively perform this projection.

13

4.1. For Method 1 (GTP-Schur):

As there is only one unknown λ_h on the interface, we need to choose λ_h piecewise constant in time on one grid, either $\mathcal{T}_1$ or $\mathcal{T}_2$. For instance, let $\lambda_h = (\lambda_h^m)_{m=1}^{M_1} \in P_0(\mathcal{T}_1, \Lambda_h)$. The fully discrete counterpart of (3.11) is weakly enforced over the time intervals of $\mathcal{T}_1$ as follows: $\forall m = 1, \ldots, M_1$,

$$\int_{J_{1,m}} \int_{\Gamma} \left(-\boldsymbol{\varphi}_{h,1}(\lambda_h, 0, 0) \cdot \boldsymbol{n}_1 - \Pi_{12} \left(\boldsymbol{\varphi}_{h,2}(\Pi_{21}(\lambda_h), 0, 0) \right) \cdot \boldsymbol{n}_1 \right) \eta_h \, d\gamma \, dt =$$

$$\int_{J_{1,m}} \int_{\Gamma} \left(\boldsymbol{\varphi}_{h,1}(0, f, c_0) \cdot \boldsymbol{n}_1 - \Pi_{12} \left(\boldsymbol{\varphi}_{h,2}(0, f, c_0) \cdot \boldsymbol{n}_1 \right) \right) \eta_h \, d\gamma \, dt, \quad \forall \eta_h \in \Lambda_h, \tag{4.3}$$

where $\boldsymbol{\varphi}_{h,i}(\lambda_h, c_0, f) = (\boldsymbol{\varphi}_{h,i}^m)_{m=1}^{M_i} \in P_0(\mathcal{T}_i, \Sigma_{h,i})$ is the solution to the fully discrete subdomain problem obtained by applying the backward Euler method to (3.10) on the time grid $\mathcal{T}_i$, $i = 1, 2$.

4.2. For Method 2 (GTO-Schwarz):

The two interface unknowns represent the Robin terms on each subdomain, thus we let $\zeta_{h,i} = (\zeta_{h,i}^m)_{m=1}^{M_i} \in P_0(\mathcal{T}_i, \Lambda_h)$. The fully discrete counterpart of (3.17) is given by

$$\int_{J_{1,m}} \int_{\Gamma} \left(\zeta_{h,1} - \Pi_{12} \left(-\boldsymbol{\varphi}_{h,2}(\zeta_{h,2}, 0, 0) \cdot \boldsymbol{n}_1 + \alpha_{1,2} \theta_{h,2}(\zeta_{h,2}, 0, 0) \right) \right) \eta_h \, d\gamma \, dt =$$

$$\int_{J_{1,m}} \int_{\Gamma} \Pi_{12} \left(-\boldsymbol{\varphi}_{h,2}(0, f, c_0) \cdot \boldsymbol{n}_1 + \alpha_{1,2} \theta_{h,2}(0, f, c_0) \right) \eta_h \, d\gamma \, dt, \ \forall \eta_h \in \Lambda_h, \forall m = 1, \ldots, M_1,$$

$$\tag{4.4}$$

$$\int_{J_{2,n}} \int_{\Gamma} \left(\zeta_{h,2} - \Pi_{21} \left(-\boldsymbol{\varphi}_{h,1}(\zeta_{h,1}, 0, 0) \cdot \boldsymbol{n}_2 + \alpha_{2,1} \theta_{h,1}(\zeta_{h,1}, 0, 0) \right) \right) \eta_h \, d\gamma \, dt =$$

$$\int_{J_{2,n}} \int_{\Gamma} \Pi_{21} \left(-\boldsymbol{\varphi}_{h,1}(0, f, c_0) \cdot \boldsymbol{n}_2 + \alpha_{2,1} \theta_{h,1}(0, f, c_0) \right) \eta_h \, d\gamma \, dt, \ \forall \eta_h \in \Lambda_h, \forall n = 1, \ldots, M_2.$$

$$\tag{4.5}$$

where $\theta_{h,i}(\zeta_{h,i}, c_0, f) = (\theta_{h,i}^m)_{m=1}^{M_i} \in P_0(\mathcal{T}_i, \Theta_{h,i})$ and $\boldsymbol{\varphi}_{h,i}(\zeta_{h,i}, c_0, f) = (\boldsymbol{\varphi}_{h,i}^m)_{m=1}^{M_i} \in P_0(\mathcal{T}_i, \Sigma_{h,i})$ are the solution to the fully discrete subdomain problem obtained by applying the backward Euler method to (3.16) on the associated time grid $\mathcal{T}_i$, $i = 1, 2$. We consider the fully discrete OSWR algorithm associated with (4.4)-(4.5) using Jacobi iterations and prove that this algorithm converges.

14

4.2.1. Fully discrete OSWR algorithm with nonconforming time grids

The OSWR algorithm reads as follows: at the kth iteration, we solve the following subdomain problem for $m = 1, \ldots, M_i$, and $i = 1, 2$:

$$
\left(\omega_i \frac{c_{h,i}^{k,m} - c_{h,i}^{k,m-1}}{\Delta t_{i,m}}, \mu_h \right)_{\Omega_i} + \left(\nabla \cdot \boldsymbol{\varphi}_{h,i}^{k,m}, \mu_h \right)_{\Omega_i} = (f^m, \mu_h)_{\Omega_i}, \ \forall \mu_h \in M_{h,i},
$$

$$
\left(\boldsymbol{D}_i^{-1} \boldsymbol{\varphi}_{h,i}^{k,m}, \boldsymbol{v}_h \right)_{\Omega_i} - \sum_{K \in \mathcal{T}_{h,i}} \sum_{E \subset \partial K} u_{i,KE} \, \mathcal{U}_{KE} \left(c_{i,K}^{k,m}, \theta_{i,E}^{k,m} \right) \left(\boldsymbol{D}_i^{-1} \boldsymbol{w}_{KE}, \boldsymbol{v}_h \right)_{\Omega_i}
$$

$$
- \left(\nabla \cdot \boldsymbol{v}_h, c_{h,i}^{k,m} \right)_{\Omega_i} + \sum_{K \in \mathcal{K}_h} \left\langle \theta_{h,i}^{k,m}, \boldsymbol{v}_h \cdot \boldsymbol{n}_K \right\rangle_{\partial K} = 0, \quad \forall \boldsymbol{v}_h \in \Sigma_{h,i},
$$

$$
\sum_{K \in \mathcal{K}_h} \left(\vartheta_h, \boldsymbol{\varphi}_{h,i}^{k,m} \cdot \boldsymbol{n}_K \right)_{\partial K} = 0, \ \forall \vartheta_h \in \Theta_h^{\Gamma,0},
$$

$$
\Delta t_{i,m} \int_\Gamma \left(-\boldsymbol{\varphi}_{h,i}^{k,m} \cdot \boldsymbol{n}_i + \alpha_{i,j} \theta_{h,i}^{k,m} \right) \eta_h \, d\gamma \, dt
$$

$$
= \int_{J_{i,m}} \int_\Gamma \Pi_{ij} \left(-\boldsymbol{\varphi}_{h,j}^{k-1} \cdot \boldsymbol{n}_i + \alpha_{i,j} \theta_{h,j}^{k-1} \right) \eta_h \, d\gamma \, dt, \quad \forall \eta_h \in \Lambda_h,
$$

$$
(c_{h,i}^{k,0}, \mu_h)_{\Omega_i} = (c_0, \mu_h)_{\Omega_i}, \quad \forall \mu_h \in M_{h,i}.
$$

(4.6)

Theorem 4.1. *Assume that $\alpha_{1,2} = \alpha_{2,1} > 0$. Algorithm (4.6), initialized by $(g_{i,j})$ in $P_0(\mathcal{T}_i; \Lambda_h)$ for $i = 1, 2$, $j = 3 - i$, defines a unique sequence of iterates*

$$
\left(c_{h,i}^k, \boldsymbol{\varphi}_{h,i}^k, \theta_{h,i}^k \right) \in P_0(\mathcal{T}_i; M_{h,i}) \times P_0(\mathcal{T}_i; \Sigma_{h,i}) \times P_0(\mathcal{T}_i; \Theta_{h,i}),
$$

that converges, for h sufficiently small, to the solution of the problem

$$
\left(\omega_i \frac{c_{h,i}^m - c_{h,i}^{m-1}}{\Delta t_{i,m}}, \mu_h \right)_{\Omega_i} + \left(\nabla \cdot \boldsymbol{\varphi}_{h,i}^m, \mu_h \right)_{\Omega_i} = (f^m, \mu_h)_{\Omega_i}, \ \forall \mu_h \in M_{h,i},
$$

$$
\left(\boldsymbol{D}_i^{-1} \boldsymbol{\varphi}_{h,i}^m, \boldsymbol{v}_h \right)_{\Omega_i} - \sum_{K \in \mathcal{T}_{h,i}} \sum_{E \subset \partial K} u_{i,KE} \, \mathcal{U}_{KE} \left(c_{i,K}^m, \theta_{i,E}^m \right) \left(\boldsymbol{D}_i^{-1} \boldsymbol{w}_{KE}, \boldsymbol{v}_h \right)_{\Omega_i}
$$

$$
- \left(\nabla \cdot \boldsymbol{v}_h, c_{h,i}^m \right)_{\Omega_i} + \sum_{K \in \mathcal{K}_h} \left\langle \theta_{h,i}^m, \boldsymbol{v}_h \cdot \boldsymbol{n}_K \right\rangle_{\partial K} = 0, \quad \forall \boldsymbol{v}_h \in \Sigma_{h,i},
$$

$$
\sum_{K \in \mathcal{K}_h} \left(\vartheta_h, \boldsymbol{\varphi}_{h,i}^m \cdot \boldsymbol{n}_K \right)_{\partial K} = 0, \ \forall \vartheta_h \in \Theta_h^{\Gamma,0},
$$

$$
\Delta t_{i,m} \int_\Gamma \left(-\boldsymbol{\varphi}_{h,i}^m \cdot \boldsymbol{n}_i + \alpha_{i,j} \theta_{h,i}^m \right) \eta_h \, d\gamma \, dt
$$

$$
= \int_{J_{i,m}} \int_\Gamma \Pi_{ij} \left(-\boldsymbol{\varphi}_{h,j} \cdot \boldsymbol{n}_i + \alpha_{i,j} \theta_{h,j} \right) \eta_h \, d\gamma \, dt, \quad \forall \eta_h \in \Lambda_h,
$$

$$
(c_{h,i}^0, \mu_h)_{\Omega_i} = (c_0, \mu_h)_{\Omega_i}, \quad \forall \mu_h \in M_{h,i},
$$

(4.7)

for $m = 1, \ldots, M_i$, and $i = 1, 2$.

Remark 4.2. *For simplicity, we present the convergence theorem for the case of two subdomains. However, the result still holds for a decomposition into multiple nonoverlapping subdomains Ω_i for $i = 1, 2, \ldots, I$ and under the assumption $\alpha_{i,j} = \alpha_{j,i}$ for $i = 1, 2, \ldots, I$ and $j \in \mathcal{N}_i$, where $\mathcal{N}_i$ denotes the set of indices of the neighbors of the subdomain Ω_i.*

Proof. As the equations are linear, we take $f = 0$ and $c_0 = 0$ and prove the sequence of iterates converges to zero. We first derive an estimate for the errors $\|\theta_{h,i}\|_{0,E}$ on the edges. Following the techniques in [5], for $K \in \mathcal{K}_h$ and $E \subset \partial K$ there exists a unique $\boldsymbol{\tau}_E \in \Sigma_{h,i}$ such that $\text{supp}(\boldsymbol{\tau}_E) \subseteq K$ and

$$\boldsymbol{\tau}_E \cdot \boldsymbol{n}_{E'} = \begin{cases} \theta_{h,i}^{k,m} & \text{if } E = E', \\ 0 & \text{otherwise.} \end{cases}$$

By a scaling argument, we obtain

$$h_K \|\boldsymbol{\tau}_E\|_{1,K} + \|\boldsymbol{\tau}\|_{0,K} \leq C h_K^{1/2} \|\theta_{h,i}^{k,m}\|_{0,E}, \tag{4.8}$$

where C (here and in the following) denotes a generic positive constant which is independent of the mesh size and time step size. Proceeding as in [13], we take $\boldsymbol{v}_h = \boldsymbol{\tau}_E$ in $(4.6)_2$, then use (4.8), the uniform ellipticity of $\boldsymbol{D}^{-1}$ and the uniform boundedness of $\boldsymbol{u}$, and divide both sides by $\|\theta_{h,i}^{k,m}\|_{0,E}$ to obtain, for $E \subset \partial K$:

$$\|\theta_{h,i}^{k,m}\|_{0,E} \leq C \left(h_K^{1/2} \|\boldsymbol{\varphi}_{h,i}^{k,m}\|_{0,K} + h_K^{-1/2} \|c_{h,i}^{k,m}\|_{0,K} + h_K^{1/2} \sum_{E' \subset \partial K} |E'|(|c_{i,K}^{k,m}| + |\theta_{i,E'}^{k,m}|) \right)$$

$$\leq C \left(h_K^{1/2} \|\boldsymbol{\varphi}_{h,i}^{k,m}\|_{0,K} + h_K^{-1/2} \|c_{h,i}^{k,m}\|_{0,K} + h_K \sum_{E' \subset \partial K} \|\theta_{i,E'}^{k,m}\|_{0,E'} \right).$$

Summing over all the edges of element K and for h sufficiently small, we deduce that

$$\|\theta_{h,i}^{k,m}\|_{0,E} \leq C \left(h_K^{1/2} \|\boldsymbol{\varphi}_{h,i}^{k,m}\|_{0,K} + h_K^{-1/2} \|c_{h,i}^{k,m}\|_{0,K} \right). \tag{4.9}$$

Next, we choose $\mu_h = c_{h,i}^{k,m}$, $\boldsymbol{v}_h = \boldsymbol{\varphi}_{h,i}^{k,m}$ and $\mu_h = \theta_{h,i}^{k,m}$ in the first three equations of (4.6), then add the resulting equations:

$$\left(\omega_i c_{h,i}^{k,m}, c_{h,i}^{k,m} \right)_{\Omega_i} - \left(\omega_i c_{h,i}^{k,m-1}, c_{h,i}^{k,m} \right)_{\Omega_i} + \Delta t_{i,m} \left(\boldsymbol{D}_i^{-1} \boldsymbol{\varphi}_{h,i}^{k,m}, \boldsymbol{\varphi}_{h,i}^{k,m} \right)_{\Omega_i}$$

$$- \Delta t_{i,m} \sum_{K \in \mathcal{T}_{h,i}} \sum_{E \subset \partial K} u_{i,KE} \, \mathcal{U}_{KE} \left(c_{i,K}^{k,m}, \theta_{i,E}^{k,m} \right) \left(\boldsymbol{D}_i^{-1} \boldsymbol{w}_{KE}, \boldsymbol{\varphi}_{h,i}^{k,m} \right)_{\Omega_i}$$

$$+ \Delta t_{i,m} \int_\Gamma \theta_{h,i}^{k,m} \left(\boldsymbol{\varphi}_{h,i}^{k,m} \cdot \boldsymbol{n}_i \right) d\gamma = 0.$$

16

Replacing the interface term by using the following equation

$$
\left(-\boldsymbol{\varphi}_{h,i}^{k,m} \cdot \boldsymbol{n}_i + \alpha_{i,j}\theta_{h,i}^{k,m}\right)^2 - \left(-\boldsymbol{\varphi}_{h,i}^{k,m} \cdot \boldsymbol{n}_i - \alpha_{j,i}\theta_{h,i}^{k,m}\right)^2
$$
$$
= 2\left(\alpha_{i,j} + \alpha_{j,i}\right)\theta_{h,i}^{k,m}\left(-\boldsymbol{\varphi}_{h,i}^{k,m} \cdot \boldsymbol{n}_i\right) + (\alpha_{i,j}^2 - \alpha_{j,i}^2)\left(\theta_{h,i}^{k,m}\right)^2, \tag{4.10}
$$

we obtain

$$
\left(\omega_i c_{h,i}^{k,m}, c_{h,i}^{k,m}\right)_{\Omega_i} - \left(\omega_i c_{h,i}^{k,m-1}, c_{h,i}^{k,m}\right)_{\Omega_i} + \Delta t_{i,m}\left(\boldsymbol{D}_i^{-1}\boldsymbol{\varphi}_{h,i}^{k,m}, \boldsymbol{\varphi}_{h,i}^{k,m}\right)_{\Omega_i}
$$
$$
-\Delta t_{i,m}\sum_{K\in\mathcal{T}_{h,i}}\sum_{E\subset\partial K} u_{i,KE}\,\mathcal{U}_{KE}\left(c_{i,K}^{k,m}, \theta_{i,E}^{k,m}\right)\left(\boldsymbol{D}_i^{-1}\boldsymbol{w}_{KE}, \boldsymbol{\varphi}_{h,i}^{k,m}\right)_{\Omega_i}
$$
$$
+\frac{\Delta t_{i,m}}{2(\alpha_{i,j} + \alpha_{j,i})}\int_{\Gamma}\left(-\boldsymbol{\varphi}_{h,i}^{k,m} \cdot \boldsymbol{n}_i - \alpha_{j,i}\theta_{h,i}^{k,m}\right)^2 d\gamma
$$
$$
=\frac{\Delta t_{i,m}}{2(\alpha_{i,j} + \alpha_{j,i})}\int_{\Gamma}\left(-\boldsymbol{\varphi}_{h,i}^{k,m} \cdot \boldsymbol{n}_i + \alpha_{i,j}\theta_{h,i}^{k,m}\right)^2 d\gamma + \frac{\Delta t_{i,m}}{2}\int_{\Gamma}\left((\alpha_{j,i} - \alpha_{i,j})\left(\theta_{h,i}^{k,m}\right)^2\right) d\gamma. \tag{4.11}
$$

From the boundedness of $\boldsymbol{u}$, (4.9) and $|a|\,|b| \leq \varepsilon a^2 + \frac{1}{4\varepsilon}b^2$ (for any $\varepsilon > 0$), we have that

$$
\Delta t_{i,m}\sum_{K\in\mathcal{T}_{h,i}}\sum_{E\subset\partial K} u_{i,KE}\,\mathcal{U}_{KE}\left(c_{i,K}^{k,m}, \theta_{i,E}^{k,m}\right)\left(\boldsymbol{D}_i^{-1}\boldsymbol{w}_{KE}, \boldsymbol{\varphi}_{h,i}^{k,m}\right)_{\Omega_i}
$$
$$
\leq C\Delta t_{i,m}\sum_{K\in\mathcal{T}_{h,i}}\sum_{E\subset\partial K}|E|\left(|c_{i,K}^{k,m}| + |\theta_{i,E}^{k,m}|\right)\|\boldsymbol{\varphi}_{h,i}^{k,m}\|_{0,K}
$$
$$
\leq C\Delta t_{i,m}\sum_{K\in\mathcal{T}_{h,i}}\|c_{i,K}^{k,m}\|_{0,K}\|\boldsymbol{\varphi}_{h,i}^{k,m}\|_{0,K} + C\Delta t_{i,m}\sum_{K\in\mathcal{T}_{h,i}}h_K^{1/2}\sum_{E\subset\partial K}\|\theta_{i,E}^{k,m}\|_{0,E}\|\boldsymbol{\varphi}_{h,i}^{k,m}\|_{0,K}
$$
$$
\leq C\Delta t_{i,m}\sum_{K\in\mathcal{T}_{h,i}}\|c_{i,K}^{k,m}\|_{0,K}\|\boldsymbol{\varphi}_{h,i}^{k,m}\|_{0,K} + C\Delta t_{i,m}\sum_{K\in\mathcal{T}_{h,i}}h_K\|\boldsymbol{\varphi}_{h,i}^{k,m}\|_{0,K}^2
$$
$$
\leq C\varepsilon\|c_{h,i}^{k,m}\|_{0,\Omega_i}^2 + \frac{C(\Delta t_{i,m})^2}{4\varepsilon}\|\boldsymbol{\varphi}_{h,i}^{k,m}\|_{0,\Omega_i}^2 + C\Delta t_{i,m}\,h\,\|\boldsymbol{\varphi}_{h,i}^{k,m}\|_{0,\Omega_i}^2.
$$

Using this inequality, the assumptions about ω, $\boldsymbol{D}$ and $\boldsymbol{u}$, the Cauchy-Schwarz inequality and $a^2 - ab \geq \frac{1}{2}(a^2 - b^2)$, we deduce from (4.11) that

$$
\omega_-\left(\|c_{h,i}^{k,m}\|_{0,\Omega_i}^2 - \|c_{h,i}^{k,m-1}\|_{0,\Omega_i}^2\right) + 2\delta_-\Delta t_{i,m}\|\boldsymbol{\varphi}_{h,i}^{k,m}\|_{0,\Omega_i}^2
$$
$$
+\frac{\Delta t_{i,m}}{(\alpha_{i,j} + \alpha_{j,i})}\int_{\Gamma}\left(-\boldsymbol{\varphi}_{h,i}^{k,m} \cdot \boldsymbol{n}_i - \alpha_{j,i}\theta_{h,i}^{k,m}\right)^2 d\gamma
$$
$$
\leq \frac{\Delta t_{i,m}}{(\alpha_{i,j} + \alpha_{j,i})}\int_{\Gamma}\left(-\boldsymbol{\varphi}_{h,i}^{k,m} \cdot \boldsymbol{n}_i + \alpha_{i,j}\theta_{h,i}^{k,m}\right)^2 d\gamma + \frac{\Delta t_{i,m}}{2}\int_{\Gamma}\left((\alpha_{j,i} - \alpha_{i,j})\left(\theta_{h,i}^{k,m}\right)^2\right) d\gamma
$$
$$
+C\varepsilon\|c_{h,i}^{k,m}\|_{0,\Omega_i}^2 + \frac{C(\Delta t_{i,m})^2}{4\varepsilon}\|\boldsymbol{\varphi}_{h,i}^{k,m}\|_{0,\Omega_i}^2 + C\Delta t_{i,m}\,h\,\|\boldsymbol{\varphi}_{h,i}^{k,m}\|_{0,\Omega_i}^2.
$$

17

As $c_{h,i}^k, \boldsymbol{\varphi}_{h,i}^k$ and $\theta_{h,i}^k$ are piecewise constant on each time interval $J_{i,m}$ and as $\alpha_{i,j} = \alpha_{j,i}$ we have

$$C_\omega \left(\|c_{h,i}^{k,m}\|_{0,\Omega_i}^2 - \|c_{h,i}^{k,m-1}\|_{0,\Omega_i}^2 \right) + C_\delta \int_{J_{i,m}} \|\boldsymbol{\varphi}_{h,i}^k\|_{0,\Omega_i}^2 \, dt$$

$$+ \frac{1}{(\alpha_{i,j} + \alpha_{j,i})} \int_{J_{i,m}} \int_\Gamma \left(-\boldsymbol{\varphi}_{h,i}^k \cdot \boldsymbol{n}_i - \alpha_{j,i}\theta_{h,i}^k \right)^2 \, d\gamma \, dt$$

$$\leq \frac{1}{(\alpha_{i,j} + \alpha_{j,i})} \int_{J_{i,m}} \int_\Gamma \left(-\boldsymbol{\varphi}_{h,i}^k \cdot \boldsymbol{n}_i + \alpha_{i,j}\theta_{h,i}^k \right)^2 \, d\gamma \, dt,$$

where $C_\omega = \omega_- - C\varepsilon$ and $C_\delta = 2\delta_- - \dfrac{C\Delta t_{i,m}}{4\varepsilon} - Ch$, which are positive for sufficiently small $\varepsilon, \Delta t_{i,m}$ and h. We sum over all the subintervals $J_{i,m}$ and using $(4.6)_4$ to obtain

$$C_\omega \|c_{h,i}^{k,M_i}\|_{0,\Omega_i}^2 + C_\delta \int_0^T \|\boldsymbol{\varphi}_{h,i}^k\|_{0,\Omega_i}^2 \, dt + \frac{1}{(\alpha_{i,j} + \alpha_{j,i})} \int_0^T \int_\Gamma \left(-\boldsymbol{\varphi}_{h,i}^k \cdot \boldsymbol{n}_i - \alpha_{j,i}\theta_{h,i}^k \right)^2 \, d\gamma \, dt$$

$$\leq \frac{1}{(\alpha_{i,j} + \alpha_{j,i})} \int_0^T \int_\Gamma \left(\Pi_{ij}(-\boldsymbol{\varphi}_{h,j}^{k-1} \cdot \boldsymbol{n}_i + \alpha_{i,j}\theta_{h,j}^k) \right)^2 \, d\gamma \, dt$$

$$\leq \frac{1}{(\alpha_{i,j} + \alpha_{j,i})} \int_0^T \int_\Gamma \left(-\boldsymbol{\varphi}_{h,j}^{k-1} \cdot \boldsymbol{n}_i + \alpha_{i,j}\theta_{h,j}^{k-1} \right)^2 \, d\gamma \, dt,$$

$$(4.12)$$

where the last inequality is obtained due to the fact that Π_{ij} is an L^2 projection. Define for $k \geq 1$

$$B^k = \sum_{i=1}^2 \int_0^T \int_\Gamma \left(-\boldsymbol{\varphi}_{h,j}^k \cdot \boldsymbol{n}_i + \alpha_{i,j}\theta_{h,j}^k \right)^2 \, d\gamma \, dt, \quad j = 3 - i,$$

and sum (4.12) over the subdomains $i = 1, 2$, we deduce that

$$C_\omega \|c_{h,i}^{k,M_i}\|_{0,\Omega_i}^2 + C_\delta \int_0^T \|\boldsymbol{\varphi}_{h,i}^k\|_{0,\Omega_i}^2 \, dt + B^k \leq B^{k-1}. \tag{4.13}$$

We sum over the iterates k to obtain $\|c_{h,i}^{k,M_i}\|_{0,\Omega_i}^2$ and $\displaystyle\int_0^T \|\boldsymbol{\varphi}_{h,i}^k\|_{0,\Omega_i}^2 \, dt$ converge to zero as $k \to \infty$. As $\boldsymbol{\varphi}_{h,i}^k \in P_0(\mathcal{T}_i; \Sigma_{h,i})$, the latter implies that $\|\boldsymbol{\varphi}_{h,i}^{k,m}\|_{0,\Omega_i}^2$ converges to zero as $k \to \infty$ for $m = 1, \ldots, M_i$. Finally, it can be shown that $\|c_{h,i}^{k,m}\|_{0,\Omega_i}^2$ converges to zero for all $m = 1, \ldots, M_i$, and $i = 1, 2$ by taking $\mu_h = c_h^{m-1}$ in $(4.6)_1$.

To prove the well-posedness of a solution to (4.6), it suffices to show uniqueness which is obtained by noting that (4.13) still holds without the superscript k. $\quad\square$

Remark 4.3. *For the fully discrete problems with nonconforming time grids and global-in-time projections, we need to assume $\alpha_{i,j} = \alpha_{j,i}$ to perform theoretical convergence analysis. This condition is not necessary for the semi-discrete case since we can use Gronwall's lemma as in [34]. For numerical experiments, different Robin parameters still lead to convergence of the iterative algorithms.*

5. Numerical experiments

We present three test cases to study and compare the performance of the GTP-Schur and GTO-Schwarz methods proposed in the previous sections. In all numerical experiments, we consider $\boldsymbol{D} = d\boldsymbol{I}$ isotropic and constant on each subdomain, where $\boldsymbol{I}$ is the 2D identity matrix. Consequently, we may denote by d_i, the diffusion coefficient in the subdomains. For the first two test cases, we consider a decomposition into two subdomains. In Test case 1, the same constant coefficients are used in the subdomains, while in Test case 2, discontinuous coefficients are used with different Peclét numbers to check the robustness of the methods when advection is dominant. Test case 3 is a prototype for the simulation of the transport around a surface nuclear waste storage where the geometry of the computational domain is complex and the physical coefficients are highly variable. The domain is decomposed into six subdomains and time windows are used for long time simulations.

We aim to investigate the accuracy and the convergence speed of the iterative algorithms. Particularly, we will verify the performance of Neumann-Neumann preconditioner for GTP-Schur and optimized parameters for GTO-Schwarz. Following the work in [43] for elliptic problems with strong heterogeneities, we use the following formula to calculate the weights $\sigma_{i,j}$ in (3.12) for the Neumann-Neumann preconditioner:

$$\sigma_{i,j} = \left(\frac{d_i}{d_i + d_j} \right)^2, \ i = 1, 2, \dots, I, \ j \in \mathcal{N}_j.$$

Numerically, it has been observed in [34, 37] that such a choice also leads to a good performance for time-dependent problems with large jumps in the coefficients between the subdomains. For GTO-Schwarz, we use two-sided optimized Robin parameters, i.e. $\alpha_{i,j} \neq \alpha_{j,i}$, obtained by numerically minizing the continuous convergence factor of the OSWR algorithm [23, 32]. We remark that for the case with a rotating velocity field [48], the GTO-Schwarz method still works well as numerically investigated in [22, 45] (with primal formulations) and in [34, Chapter 3]) (with mixed formulations and operator splitting).

5.1. Test case 1: with a known analytical solution

We first verify the accuracy in space and in time of the proposed algorithms by considering a test case with the exact solution is given by

$$u(x, y, t) = e^{-4t} \sin(\pi x) \sin(\pi y),$$

on the unit square $\Omega = (0,1)^2$. We split Ω into two nonoverlapping subdomains $\Omega_1 = (0, 0.5) \times (0, 1)$ and $\Omega_2 = (0.5, 1) \times (0, 1)$. Constant parameters are imposed on the whole domain: $\omega_i = 1$, $\boldsymbol{u}_i = (1, \ 1)^T$, $d_i = 1$, for $i = 1, 2$. For the spatial discretization, we consider a conforming rectangular mesh with size $h_1 = h_2 = h$. For the time discretization, we use nonconforming time grids with $\Delta t_1 \neq \Delta t_2$. The interface problem associated with each method is solved iteratively by GMRES with a zero initial guess on the interface; the iteration stops when the relative residual is smaller than 10^{-6}.

In Table 1, we show the relative $L^2(\Omega)$−norm errors of c and $\boldsymbol{\varphi}$ at $T = 0.1$ with fixed time step sizes $\Delta t_1 = T/80$ and $\Delta t_2 = T/60$ and a decreasing mesh size h. The number of subdomain solves are also reported for the global-in-time Schur (GT-Schur) method with or without Neumann-Neumann preconditioner and the GTO-Schwarz method with optimized parameters. Note that one iteration of the GT-Schur method with the preconditioner costs twice as much as one iteration of the GTO-Schwarz method (in terms of number of subdomain solves), thus we show the number of subdomain solves (instead of number of iterations) to compare the two methods. We observe that the errors by both methods are almost identical, and the order of accuracy in space is preserved with nonconforming time grids. For GT-Schur, the preconditioner significantly improves the convergence speed, and the convergence is almost independent of h. GTO-Schwarz converges a little slower than GT-Schur for this case, and the number of GMRES iterations increases slightly when h is decreasing. Note that for steady-state problems [20], the convergence factor of the optimized Schwarz algorithm (i.e. Jacobi iterations) behaves like $1 - O(h^{1/4})$.

| | Method 1: GT-Schur | | | | Method 2: GTO-Schwarz | | |
| | L^2 errors | | # subdomain solves | | L^2 errors | | # subdomain |
h	c	$\boldsymbol{\varphi}$	No Precond.	With Precond.	c	$\boldsymbol{\varphi}$	solves
1/20	0.0641	0.0453	29	12	0.0641	0.0454	16
1/40	0.0321 [1.00]	0.0227 [1.00]	39	12	0.0321 [1.00]	0.0227 [1.00]	16
1/80	0.0160 [1.00]	0.0114 [0.99]	54	12	0.0160 [1.00]	0.0114 [0.99]	20
1/160	0.0080 [1.00]	0.0057 [1.00]	76	14	0.0080 [1.00]	0.0058 [0.98]	22

Table 1: [Test case 1] Accuracy in space, the convergence rates are shown in square brackets.

In Table 2, we show the relative $L^2(\Omega)$−norm errors of c and $\boldsymbol{\varphi}$ at $T = 1$ with fixed $h = 1/200$ and decreasing time step sizes $\Delta t_1 = {}^3\!/\!{}_4 \Delta t_2$. The accuracy in time is preserved with nonconforming time grids. In addition, the errors obtained by the two methods are not the same, especially when the time step sizes are large. This is due to the use of different projection operators, which makes the two methods yield different solutions at convergence (cf. Section 4). However, as Δt_i, $i = 1, 2$, become smaller, numerical results suggest that the two methods converge to the same continuous-in-time solution. Again, the preconditioner as well as optimized parameters work well in terms of convergence speed.

| | Method 1: GT- Schur | | | | Method 2: GTO-Schwarz | | |
| | L^2 errors | | # subdomain solves | | L^2 errors | | # subdomain |
Δt_2	c	$\boldsymbol{\varphi}$	No Precond.	With Precond.	c	$\boldsymbol{\varphi}$	solves
$T/6$	0.1186	0.1315	83	14	0.2524	0.2712	18
$T/12$	0.0520 [1.19]	0.0579 [1.18]	83	14	0.0922 [1.45]	0.1042 [1.38]	18
$T/24$	0.0251 [1.05]	0.0277 [1.06]	93	14	0.0369 [1.32]	0.0422 [1.30]	20
$T/48$	0.0134 [0.91]	0.0141 [0.97]	104	14	0.0160 [1.21]	0.0173 [1.29]	24

Table 2: [Test case 1] Accuracy in time, the convergence rates are shown in square brackets.

5.2. Test case 2: with piecewise discontinuous coefficients

Next, we analyze the convergence of the iterative algorithms. Towards that end, we consider the error equation with the same two nonoverlapping subdomains as in Test case 1. The porosity is $\omega_1 = \omega_2 = \omega = 1$. The diffusion and advection coefficients, d_i and $\boldsymbol{u}_i$ for $i = 1, 2$, are constant in each subdomain and discontinuous across the interface. Their values are given in Table 3 for the diffusion dominant, mixed regime and advection dominant problems, respectively. Note that the global Péclet number in each subdomain is computed by

$$\text{Pe}_{G,i} := \frac{H \mid \boldsymbol{u}_i \mid}{d_i}, \ i = 1, 2,$$

where H is the size of the domain (in this case, $H = 1$). In space, we use a conforming rectangular mesh $h = 1/100$; in time, nonconforming time grids are considered with $\Delta t_1 = {}^3/_4 \Delta t_2$ and $\Delta t_2 = 1/75$.

Problems	d_1	$\boldsymbol{u}_1$	$\text{Pe}_{G,1}$	d_2	$\boldsymbol{u}_2$	$\text{Pe}_{G,2}$
(a) Diffusion dominance	1	$(-0.02, \ -0.5)^T$	≈ 0.5	0.1	$(-0.02, \ -0.05)^T$	≈ 0.5
(b) Mixed regime	0.01	$(-0.02, \ -0.5)^T$	≈ 50	0.1	$(-0.02, \ -0.05)^T$	≈ 0.5
(c) Advection dominance	0.02	$(0.5, \ 1)^T$	≈ 56	0.002	$(0.5, \ 0.1)^T$	≈ 255

Table 3: [Test case 2] Data for the discontinuous test case.

Figure 2 show the errors (in logarithmic scale) in $L^2(\Omega)-$norm of the flux variable $\boldsymbol{\varphi}$ versus the number of subdomain solves using GMRES with a random initial guess (similar convergence curves are obtained for the scalar variable c, and are omitted). Three algorithms are considered: GT-Schur with no preconditioner (magenta, circle), GT-Schur with the preconditioner (red, x-mark) and GTO-Schwarz (blue, triangle). We observe that for GT-Schur, the preconditioner works well in the case the Peclét number is not so large. (i.e. Problems (a) and (b) in Table 3). When the Peclét number is sufficiently large (i.e. Problem (c)), the convergence of GT-Schur with or without preconditioner is quite the same. For GTO-Schwarz, the convergence speed does not significantly change with the Peclét number. GT-Schur with the preconditioner is comparable with GTO-Schwarz when diffusion is dominant. When advection is dominant, GTO-Schwarz converges faster than GT-Schur with or without preconditioner (at least by a factor of 2.17). We remark that when operator splitting is used as in [37, 33], the GT-Schur approach with the preconditioner converges even slower than without preconditioner when advection is dominant (cf. Figure 3 in [37] and Figure 3.8 in [33, Chapter 3] where the Peclét numbers are approximately 100 and $100\sqrt{2}$ respectively).

To verify the performance of the optimized parameters, we show in Figure 3 the relative residuals (in logarithmic scale) for various values of the parameters $\alpha_{1,2}$ and $\alpha_{2,1}$ after a fixed number of Jacobi iterations. We see that for different sets of parameters, the pair of optimized Robin parameters (red star) is located close to those giving the smallest relative residual after the same number of iterations.
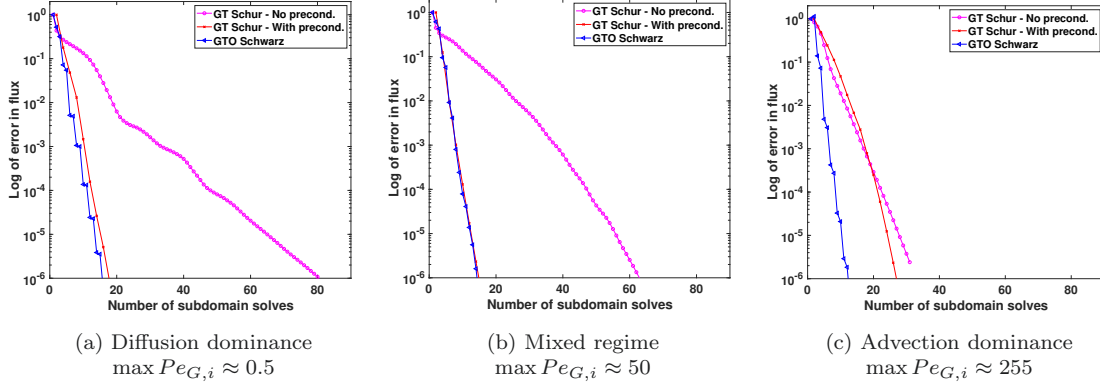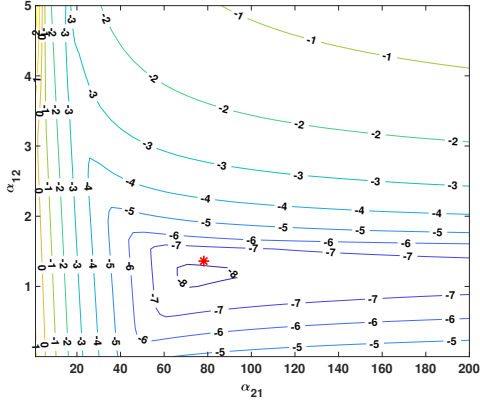
(a) Diffusion dominance
max $Pe_{G,i} \approx 0.5$

(b) Mixed regime
max $Pe_{G,i} \approx 50$

(c) Advection dominance
max $Pe_{G,i} \approx 255$

Figure 2: [Test case 2] Convergence curves by GMRES for different Péclet numbers: L^2-norm errors in the flux $\boldsymbol{\varphi}$ at $T = 1$ for Method 1 (GT-Schur) with no preconditioner (magenta curves) and with the Neumann-Neumann preconditioner (red curves), and Method 2 (GTO-Schwarz) (blue curves).

We now investigate whether the nonconforming time grids preserve the accuracy in time. We consider the advection dominant problem (i.e. Problem (c)) with the same coefficients given in Table 3. Homogeneous Dirichlet conditions are imposed on the boundary, the source term is $f(x, y, t) = \exp(-100((x - 0.2)^2 + (y - 0.2)^2))$, and the initial condition $p_0(x, y) = xy(1 - x)(1 - y) \exp(-100((x - 0.2)^2 + (y - 0.2)^2))$. We use four initial time grids with $\Delta t_c = T/12$ and $\Delta t_f = T/16$ where $T = 0.5$:

- Time grid 1 (coarse-coarse): conforming with $\Delta t_1 = \Delta t_2 = \Delta t_c$.
- Time grid 2 (coarse-fine): nonconforming with $\Delta t_1 = \Delta t_c$ and $\Delta t_2 = \Delta t_f$.
- Time grid 3 (fine-coarse): nonconforming with $\Delta t_1 = \Delta t_f$ and $\Delta t_2 = \Delta t_c$.
- Time grid 4 (fine-fine): conforming with $\Delta t_1 = \Delta t_2 = \Delta t_f$.

The time steps are then refined several times by a factor of 2. In space, we fix a conforming rectangular mesh with $h = 1/200$, and we compute a reference solution by solving problem (2.5) directly on a very fine time grid, with $\Delta t = \Delta t_f/2^7$. The converged DD solution is such that the relative residual is smaller than 10^{-8}. We show in Figure 4 the relative errors at $T = 0.5$ versus the time step $\Delta t = \max(\Delta t_c, \Delta t_f)$. We only give the results for GTP-Schur because the curves for GTO-Schwarz look exactly the same. We observe that first order convergence is preserved in the nonconforming case. The errors obtained in the nonconforming case with a fine time step in Ω_1 where the parameters are large (Time grid 3 with blue triangle markers) are nearly the same as in the finer conforming case (Time grid 4, in red with circle markers). On the other hand, the errors obtained in the nonconforming case with a fine time step in Ω_2 where the parameters are small (Time grid 2 with green x-markers) are close to those by the coarse conforming case (Time grid 1,

(a) Diffusion dominance
25 Jacobi iterations
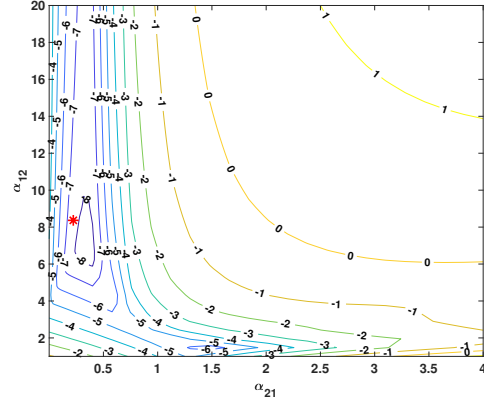
(b) Mixed regime
25 Jacobi iterations
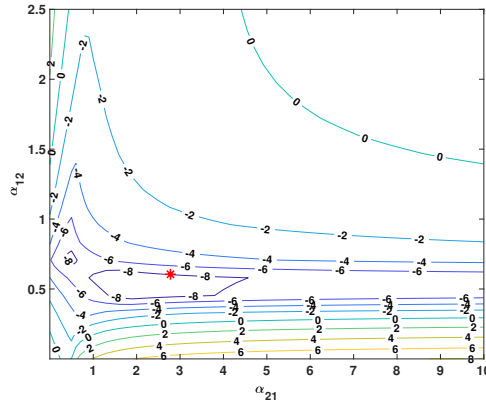
(c) Advection dominance
20 Jacobi iterations

Figure 3: [Test case 2] Level curves for the relative residuals (in logarithmic scales) after a fixed number of Jacobi iterations for various values of $\alpha_{1,2}$ and $\alpha_{2,1}$. The red star shows the optimized values computed by numerically minimizing the continuous convergence factor of the OSWR algorithm.

in magenta with diamond markers). Thus using nonconforming grids can adapt the time steps in the subdomains depending on the physical parameters and limit the computational cost locally, while preserving almost the same accuracy as in the finer conforming case.

5.3. Test case 3: A simulation for a surface, nuclear waste storage

Finally, we consider a test case introduced in [37] and designed by ANDRA[2] as a protype for simulating a surface storage of short half-life nuclear waste. The computational domain

---

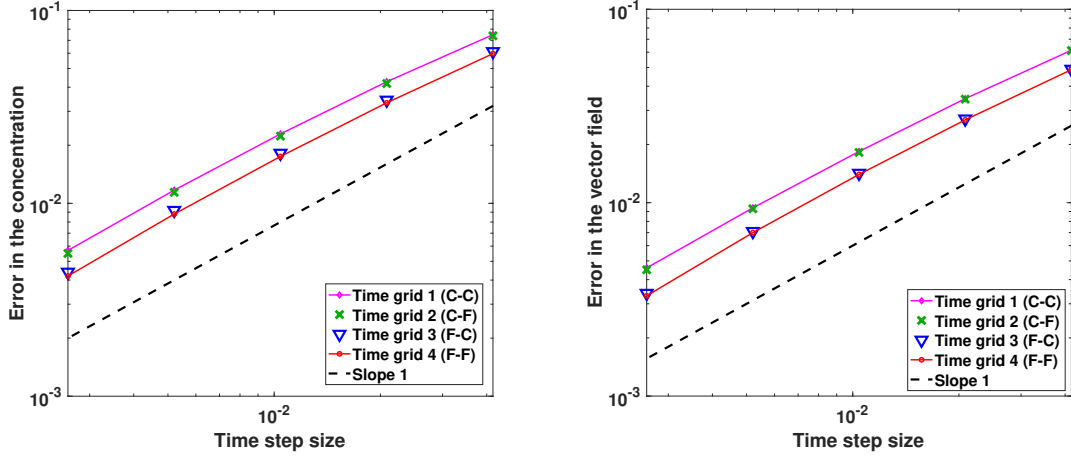[2]The French agency for nuclear waste management

Figure 4: [Test case 2] Errors in the concentration c (left) and the vector field $\boldsymbol{\varphi}$ (right) between the reference and multidomain solutions.

is depicted in Figure 5 with different physical zones, where the waste is stored in square boxes ("dechet" zone). The properties of these zones are given in Table 4. Note that in our calculation, we use the effective diffusion, defined by $d_{\text{eff}} = \omega \times d_{\text{m}}$. The advection field is governed by Darcy's law together with the law of mass conservation:

$$\begin{aligned} \boldsymbol{u} &= -K\nabla\mathfrak{h} && \text{in } \Omega, \\ \operatorname{div}\boldsymbol{u} &= 0 && \text{in } \Omega, \end{aligned} \tag{5.1}$$

where $\mathfrak{h}$ is the hydraulic head field, $\boldsymbol{u}$ is the Darcy velocity and K is the hydraulic conductivity. Dirichlet conditions are imposed on top, $\mathfrak{h} = 10\text{m}$ and on bottom $\mathfrak{h} = 9.998\text{m}$ of the domain and no flow boundary on the left and right sides. For the transport problem, the final time is $T_f = 500$ years, the source term is $f = 0$ and the initial condition is such that

$$c_0 = \begin{cases} 1, & \text{in "dechet1" and "dechet2",} \\ 0, & \text{elsewhere.} \end{cases}$$

Boundary conditions of the transport problem are homogeneous Dirichlet conditions on top and bottom, and homogeneous Neumann conditions on the left and right hand sides. For the spatial discretization of both flow and transport problems, a non-uniform rectangular mesh is used as shown in Figure 5 in blue, with 171 cells in the $x-$direction and 158 cells in the $y-$direction. The mesh size is $h \approx 0.42\text{m}$. The Darcy flow problem (5.1) is solved by using the same mixed hybrid finite element method as presented in Section 2. Numerical approximation of the hydraulic head is shown in Figure 6 (left). For the transport problem, we decompose the domain into 6 rectangular subdomains in such a way that the black zone (*terrain*) is separated from the rest and subdomain Ω_3 includes the *dallerobtur*, *voile*, *radier* and a part of *drain* zones (see Figure 6 (right)). The transport is dominated by diffusion in
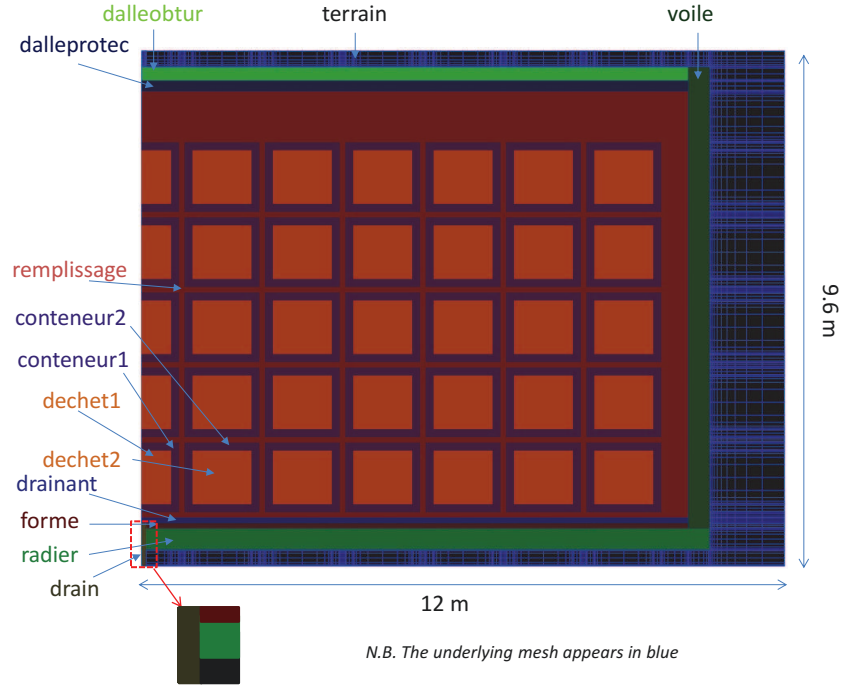
24

Figure 5: [Test case 3] The geometry of the test case [37].

Zone	Hydraulic conductivity K (m/year)	Porosity ω	Molecular diffusion d_{m} (m^2/year)
terrain	94608	0.30	1
radier	$3.1536\,10^{-4}$	0.15	$6.31\,10^{-5}$
forme	$3.1536\,10^{-3}$	0.20	$1.58\,10^{-3}$
drainant	94608	0.30	$5.36\,10^{-2}$
voile	$3.1536\,10^{-3}$	0.20	$1.58\,10^{-3}$
remplissage	5045.76	0.30	$5.36\,10^{-2}$
dalleprotec	$3.1536\,10^{-3}$	0.20	$1.58\,10^{-3}$
dalleobtur	$3.1536\,10^{-3}$	0.20	$1.58\,10^{-3}$
drain	94608	0.30	1
conteneur1/conteneur2	$3.1536\,10^{-4}$	0.12	$4.47\,10^{-4}$
dechet1/dechet2	$3.1536\,10^{-4}$	0.30	$1.37\,10^{-3}$

Table 4: [Test case 3] Data for flow and transport problems [37].

subdomain Ω_3 (the maximum of the local Péclet number $\text{Pe}_L \approx 0.0032$) and is dominated by advection (with $\text{Pe}_L \approx 2.75$) in the other subdomains.
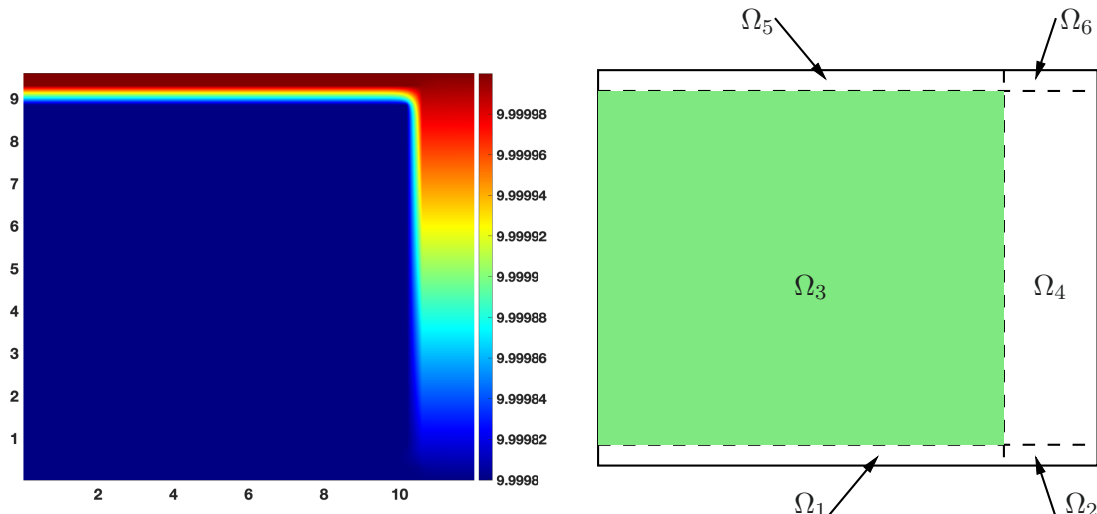

Figure 6: [Test case 3] The hydraulic head field and the decomposition of the domain.

For long time simulations, we use time windows, i.e. we split $(0, T_f)$ into nonoverlapping smaller subintervals, called time windows, and then applies the DD methods in each time window successively in which the solution from the previous time window is used as the initial guess for the next time window. For this test case, we use time windows of size $T = 5$ years, and we will first analyze the convergence behavior as well as the accuracy in time of the multidomain solution with nonconforming grids for the first time window, $(0, T)$. The time steps are $\Delta t_3 = T/50$, and $\Delta t_i = T/10$, $i \neq 3$. The interface problem is solved iteratively using GMRES with a zero initial guess for both GT-Schur and GTO-Schwarz methods, the tolerance is set to be 10^{-6}. We show in Figure 7 the relative residuals for GT-Schur with or without preconditioning and GTO-Schwarz versus the number of subdomain solves. We observe that the GTO-Schwarz method converges faster than the GT-Schur method with Neumann-Neumann preconditioner; without preconditioning, the convergence of GT-Schur is very slow and it takes more than 450 iterations to reach the same tolerance. We remark that for this test case, the advection is sufficient to make GTO-Schwarz faster than GTP-Schur with Neumann-Neumann preconditioning, but the advection term is small enough for the Neumann-Neumann preconditioner to be effective.

Next, we run the GTP-Schur (with Neumann-Neumann preconditioner) and GTO-Schwarz methods for 100 time windows and stop the iterations in each time window when the relative residual is less than 10^{-3}. The average number of iterations in each time window is approximately 8 (equivalent to 16 subdomain solves) for the GTP-Schur method and is approximately 9 (equivalent to 9 subdomain solves) for the GTO-Schwarz method. Figure 8 shows the concentration field after 20 years, 50 years, 100 years and 500 years
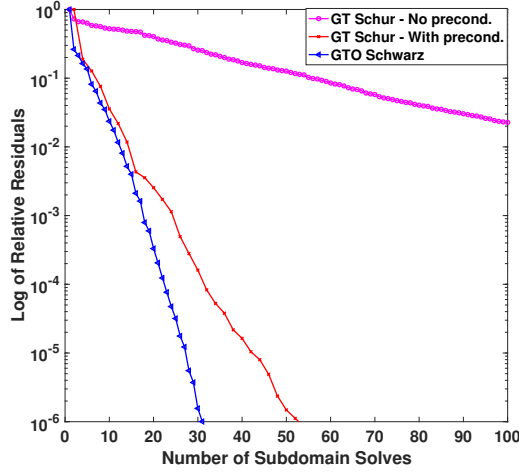
Figure 7: [Test case 3] Relative residuals of GMRES for Method 1 (GT-Schur) with no preconditioner (magenta curves) and with the Neumann-Neumann preconditioner (red curves), and Method 2 (GTO-Schwarz) (blue curves).

respectively (note that the color bar for each plot is different). We see that the radionuclide escapes from the waste packages and slowly migrates into the surrounding area. Due to the specific design of the storage and under the effect of advection, the radionuclide tends to move toward the bottom right corner.

Conclusion

We have studied two global-in-time, nonoverlapping DD methods for the linear advection-diffusion equation to model contaminant transport in heterogeneous porous media. The equation is discretized in space by a mixed hybrid method based on the lowest-order Raviart-Thomas finite element space with the flux variable consisting of both advective and diffusive flux. Lagrange multipliers are introduced to enforce the continuity of the normal flux across the inter-element boundaries and are used for the discretization of the advective term. The semi-discrete continuous-in-time problem is formulated as a space-time interface problem using either physical transmission conditions or Robin conditions, which corresponds to the GTP-Schur with Neumann-Neumann preconditioner and the GTO-Schwarz method with optimized Robin parameters, respectively. The developed methods are fully implicit in time and enable local time steps in the subdomains. This work can be seen as a sequel to [34, 37] where similar methods were studied for the pure diffusion problem and the advection-diffusion problem with operator splitting, respectively. Differently from [37], here we do not treat advection and diffusive separately and no explicit time stepping is used. We prove the convergence of the fully discrete OSWR algorithm with the upwind-mixed hybrid spatial discretization and backward Euler time-stepping method
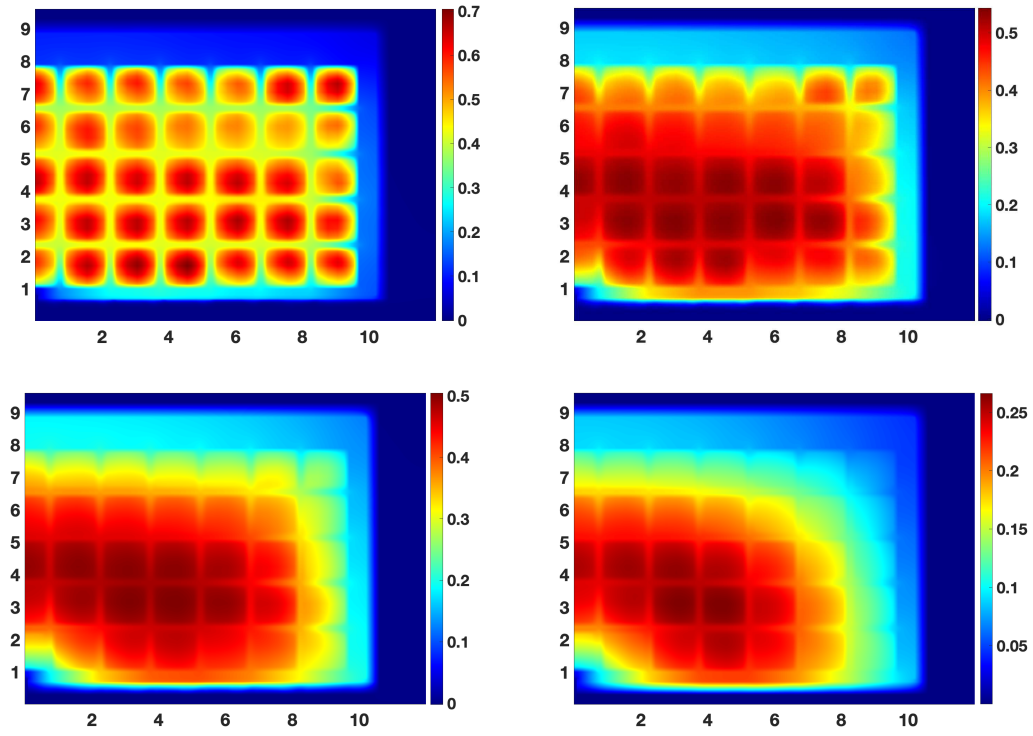
Figure 8: [Test case 3] Snapshots of the concentration after 20 years, 50 years, 100 years and 500 years respectively. The color bar for each plot is different.

on nonconforming time grids. Numerical results confirm the convergence and accuracy of the proposed methods with different time steps, and their application to long-term simulations of transport of nuclear waste around a subsurface storage. We observe that both methods handle well the case with large jumps in the coefficients, and their convergence is weakly dependent on the discretization parameters. The GTP-Schur method works well and converges faster than without a preconditioner when the advection is moderate while the GTO-Schwarz method is insensitive to the advection and converges faster than the GTP-Schur method when there is sufficient advection. We are currently investigating the GTO-Schwarz method with second-order (Ventcell) transmission conditions [35] and extension of the methods to the case of transport problems in fractured porous media as studied in [36] (for modeling the flow of a compressible fluid) where the fractures are treated as manifolds of one dimension less than the surrounding rock matrix. In addition, for GT-Schur, we plan to extend the Robin-Robin preconditioner proposed in [2, 1] for the stationary advection-diffusion equation to the time-dependent case with the mixed hybrid finite element discretization, and investigate its convergence compared to the Neumann-Neumann preconditioner for diffusion-dominated and advection-dominated problems.

References

[1] Y. ACHDOU, P. LE TALLEC, F. NATAF AND M. VIDRASCU, A domain decomposition preconditioner for an advection–diffusion problem, *Comput. Methods Appl. Mech. Engrg.* **184**, 2000, pp. 145-170.

[2] Y. ACHDOU AND F. NATAF, A Robin–Robin preconditioner for an advection–diffusion problem, *C.R. Acad. Sci. Paris* **325**, Série I, 1997, pp. 1211-1216.

[3] T. ARBOGAST, L. C. COWSAR, M. F. WHEELER AND I. YOTOV, Mixed finite element methods on nonmatching multiblock grids, *SIAM J. Numer. Anal.* **37**, 2000, pp. 1295-1315.

[4] T. ARBOGAST, G. PENCHEVA, M. F. WHEELER AND I. YOTOV, A multiscale mortar mixed finite element method, *Multiscale Model. Simul.* **6**, 2007, pp. 319-346.

[5] D. N. ARNOLD AND F. BREZZI, Mixed and nonconforming finite element methods: Implementation, postprocessing and error estimates, *RAIRO Modél. Math. Anal. Numér.* **19**, 1985, pp. 7-32.

[6] D. BENNEQUIN, M.J. GANDER, L. GOUARIN AND L.HALPERN, Optimized Schwarz waveform relaxation for advection reaction diffusion equations in two dimensions, *Numerische Mathematik* **134**(3), 2016, pp. 513-567.

[7] D. Bennequin, M.J. Gander and L. Halpern, A homographic best approximation problem with application to optimized Schwarz waveform relaxation, *Math. Comp.* **78**(265), 2009, pp.185-223.

[8] E. Blayo, L. Debreu and F. Lemarié, Toward an optimized global-in-time Schwarz algorithm for diffusion equations with discontinuous and spatially variable coefficients. Part 1: the constant coefficients case, *Electron. Trans. Numer. Anal.* **40**, 2013,pp. 170-186.

[9] E. Blayo, L. Halpern and C. Japhet, Optimized Schwarz waveform relaxation algorithms with nonconforming time discretization for coupling convection-diffusion problems with discontinuous coefficients, in Domain Decomposition Methods in Science and Engineering XVI, Lect. Notes Comput. Sci. Eng. 55, Springer, Berlin, 2007, pp. 267-274.

[10] W. M. Boon, D. Glaser, R. Helmig and I. Yotov, Flux-mortar mixed finite element methods on non-matching grids, arxiv.org/abs/2008.09372.

[11] S.C. Brenner and L.-Y. Sung, BDDC and FETI-DP without matrices or vectors, *Computer Methods in Applied Mechanics and Engineering* **196**, 2007, pp.1429-1435.

[12] F. Brezzi, and M. Fortin, *Mixed and Hybrid Finite Elements Methods*, Springer-Verlag, New York, 1991.

[13] F. Brunner, F. A. Radu and P. Knabner, Analysis of an upwind-mixed hybrid finite element method for transport problems, *SIAM J. Numer. Anal.* **52**, 2014, pp. 83-102.

[14] L. C. Cowsar, J. Mandel and M. F. Wheeler, Balancing domain decomposition for mixed finite elements, *Math. Comp.* **64**, 1995, pp. 989–1015.

[15] J.-M. Cros, A preconditioner for the Schur complement domain decomposition method, in Domain Decomposition Methods in Science and Engineering, I. Herrera, D. E. Keyes, and O. B. Widlund, eds., National Autonomous University of Mexico (UNAM), Mexico, 2003, pp. 373-380. 14th International Conference on Domain Decomposition Methods, Cocoyoc, Mexico, January 6-12, 2002.

[16] C. Dawson, Analysis of an upwind-mixed finite element method for nonlinear contaminant transport equations, *SIAM J. Numer. Anal.* **35**, 1998, pp. 1709-1724.

[17] C. R. Dohrmann, A preconditioner for substructuring based on constrained energy minimization, *SIAM J. Sci. Comput.* **25**, 2003, pp. 246-258.

[18] R. E. Ewing, R. D. Lazarov, T. F. Russell and P. S. Vassilevski, Local refinement via domain decomposition techniques for mixed finite element methods

with rectangular Raviart-Thomas elements, in Third International Symposium on Domain Decomposition Methods for Partial Differential Equations (Houston, TX, 1989), SIAM, Philadelphia, PA, 1990, pp. 98–114.

[19] Y. FRAGAKIS AND M. PAPADRAKAKIS, The mosaic of high performance domain decomposition methods for structural mechanics: Formulation, interrelation and numerical efficiency of primal and dual methods, *Comput. Methods Appl. Mech. Engrg.* **192**, 2003, pp. 3799-3830.

[20] M.J. GANDER, Optimized Schwarz methods, *SIAM J. Numer. Anal.* **44**, 2006,pp. 699-731.

[21] M.J. GANDER AND L. HALPERN, Optimized Schwarz Waveform Relaxation for Advection Reaction Diffusion Problems, *SIAM J. Numer. Anal.* **45**(2), 2007, pp. 666-697.

[22] M.J. GANDER, L. HALPERN, C. JAPHET, Optimized Schwarz Algorithms for Coupling Convection and Convection-Diffusion Problems, In N. Debit, M. Garbey, R. Hoppe, J. Périaux, D. Keyes, Y. Kuznetsov (eds.), Proceedings of the Thirteenth International Conference on Domain Decomposition Methods, pp. 253-260, 2001.

[23] M.J. GANDER, L. HALPERN AND M. KERN, A Schwarz waveform relaxation method for advection-diffusion-reaction problems with discontinuous coefficients and non-matching grids, in: Domain Decomposition Methods in Science and Engineering XVI, in: Lect. Notes Comput. Sci. Eng., vol. 55, Springer, Berlin, 2007, pp. 283–290.

[24] M. J. GANDER, L. HALPERN, AND F. NATAF, Optimal Schwarz waveform relaxation for the one dimensional wave equation, *SIAM J. Numer. Anal.* **41**, 2003, pp. 1643-1681.

[25] M.J. GANDER AND C. JAPHET, Algorithm 932: PANG: software for nonmatching grid projections in 2D and 3D with linear complexity, *ACM Trans. Math. Software* **40**, 2013, 25. Art. 6.

[26] M. J. GANDER, C. JAPHET, Y. MADAY, AND F. NATAF, A new cement to glue nonconforming grids with Robin interface conditions: The finite element case, in Domain Decomposition Methods in Science and Engineering, Lect. Notes Comput. Sci. Eng. 40, Springer, Berlin, 2005, pp. 259–266.

[27] M.J. GANDER, F. KWOK AND B.C. MANDAL, Dirichlet-Neumann and Neumann-Neumann Waveform Relaxation Algorithms for Parabolic Problems, *Electron. Trans. Numer. Anal.* **45**, 2016, pp. 424-456.

[28] M.J. GANDER, F. KWOK AND B.C. MANDAL, Dirichlet-Neumann Waveform Relaxation Methods for Parabolic and Hyperbolic Problems in Multiple Subdomains, *BIT Numerical Mathematics*, 2020, pp. 1-35.

[29] F. HAEBERLEIN, L. HALPERN AND A. MICHEL, Newton-Schwarz optimised waveform relaxation Krylov accelerators for nonlinear reactive transport, in: Domain Decomposition Methods in Science and Engineering XX, in: Lect. Notes Comput. Sci. Eng., vol. 91, Springer, Heidelberg, 2013, pp. 387–394.

[30] L. HALPERN, C. JAPHET, P. OMNES, Nonconforming in time domain decomposition method for porous media applications., in: J.C.F. Pereira, A. Sequeira (Eds.), Proceedings of the 5th European Conference on Computational Fluid Dynamics EC-COMAS CFD 2010, Lisbon, Portugal.

[31] L. HALPERN, C. JAPHET AND J. SZEFTEL, Discontinuous Galerkin and nonconforming in time optimized Schwarz waveform relaxation, in Domain Decomposition Methods in Science and Engineering XIX, Lect. Notes Comput. Sci. Eng. 78, Springer, Heidelberg, 2011, pp. 133- 140.

[32] L. HALPERN, C. JAPHET AND J. SZEFTEL, Optimized Schwarz waveform relaxation and discontinuous Galerkin time stepping for heterogeneous problems, *SIAM J. Numer. Anal.* **50**(5), 2012, pp. 2588-2611.

[33] T.T.P. HOANG, Space–time domain decomposition methods for mixed formulations of flow and transport problems in porous media (Ph.D. thesis), University Paris 6, 2013.

[34] T.T.P. HOANG, J. JAFFRÉ, C. JAPHET, M. KERN AND J.E. ROBERTS, Space-time domain decomposition methods for diffusion problems in mixed formulations, *SIAM J. Numer. Anal.* **51(6)**, 2013, pp. 3532-3559.

[35] T.T.P. HOANG, C. JAPHET, M. KERN AND J.E. ROBERTS, Ventcell Conditions with Mixed Formulations for Flow in Porous Media. In T. Dickopf, M.J. Gander, L. Halpern, R. Krause, L.F. Pavarino (eds.), Domain Decomposition Methods in Science and Engineering XXII, Lecture Notes in Computational Science and Engineering, vol. 104, pp. 531 - 540, Springer, 2016.

[36] T.T.P. HOANG, C. JAPHET, M. KERN AND J.E. ROBERTS, Space-time domain decomposition for reduced fracture models in mixed formulation *SIAM J. Numer. Anal.* **54**, 2016, pp. 288-316.

[37] T.T.P. HOANG, C. JAPHET, M. KERN AND J.E. ROBERTS, Space-Time Domain Decomposition For Advection-Diffusion Problems in Mixed Formulations, *Math. Comput. Simulat.* **137**, 2017, pp. 366-389.

[38] M. JAYADHARAN, M. KERN, M. VOHRALÍK, AND I. YOTOV, A space-time multiscale mortar mixed finite element method for parabolic equations, 2021, submitted; arxiv.org/abs/2110.02132.

[39] F. Kwok, Neumann-Neumann Waveform Relaxation for the Time-Dependent Heat Equation. In: J. Erhel, M.J. Gander, L. Halpern, G. Pichot, T. Sassi, O.B. Widlund (eds.) Domain Decomposition in Science and Engineering XXI, vol. 98, Springer-Verlag, 2014, pp. 189–198.

[40] J. Li and O. B. Widlund, FETI–DP, BDDC, and Block Cholesky Methods, *Internat. J. Numer. Methods Engrg.* **66**(2), 2006, pp.250-271.

[41] B.C. Mandal, A Time-Dependent Dirichlet-Neumann Method for the Heat Equation. In: J. Erhel, M.J. Gander, L. Halpern, G. Pichot, T. Sassi, O.B. Widlund (eds.) Domain Decomposition in Science and Engineering XXI, vol. 98, Springer-Verlag, 2014, pp. 467-475.

[42] J. Mandel, Balancing domain decomposition, *Comm. Numer. Methods Engrg.* **9**, 1993, pp. 233–241.

[43] J. Mandel and M. Brezina, Balancing domain decomposition for problems with large jumps in coefficients, *Math. Comp.* **65**, 1996, pp. 1387–1401.

[44] J. Mandel, C. R. Dohrmann and R. Tezaur, An algebraic theory for primal and dual substructuring methods by constraints, *Appl. Numer. Math.* **54**, 2005, pp. 167–193.

[45] V. Martin, An optimized Schwarz waveform relaxation method for the unsteady convection diffusion equation in two dimensions, *Appl. Numer. Math.* **52**, 2005,pp. 401-428.

[46] F. A. Radu, N. Suciu, J. Hoffmann, A. Vogel, O. Kolditz, C.-H. Park and S. Attinger, Accuracy of numerical simulations of contaminant transport in heterogeneous aquifers: A comparative study, *Adv. Water Resources* **34**, 2011, pp. 47-61.

[47] J.E. Roberts and J.M. Thomas, Mixed and hybrid methods in: *Handbook of Numerical Analysis*, Vol. II, North-Holland, Amsterdam, 1991, pp. 523-639.

[48] A. Toselli, FETI domain decomposition methods for scalar advection-diffusion problems. *Comput. Methods Appl. Mech. Engrg.* **190** (43-44), 2001, pp. 5759-5776.

[49] X. Tu, A BDDC Algorithm for Mixed Formulation of Flow in Porous Media, *Electron. Trans. Numer. Anal.* **20**, 2005, pp.164-179.